# DNA demethylation switches the drivers of Foxp3 expression to maintain regulatory T cell identity

Jun Li[1,4], Beisi Xu[2,4], Xinying Zong[1], Minghong He[1], Yiping Fan[2], Richard Cross[1], Jacob H. Hanna[3], Yongqiang Feng[1,*]

[1] Department of Immunology, St. Jude Children's Research Hospital, Memphis, TN 38105.

[2] Center for Applied Bioinformatics, St. Jude Children's Research Hospital, Memphis, TN 38105.

[3] Department of Molecular Genetics, Weizmann Institute of Science, Rehovot 7610001, Israel.

[4] These authors contributed equally.

***Correspondence:**

Yongqiang Feng: Phone 901-595-5459, Email Yong.Feng@stjude.org

**Key Words:**

Regulatory T cells, DNA demethylation, cell fate, Foxp3

## ABSTRACT

Maintenance of differentiated cellular states is crucial for numerous biological processes, yet its molecular basis remains unclear. Here, we investigate how mechanistically regulatory T ($T_{reg}$) cell fate is "locked in" during lineage commitment via transcriptional regulation of its lineage-specifying factor Foxp3. Tet-mediated DNA demethylation of *Foxp3* enhancer CNS2 was proposed to be a key mechanism maintaining Foxp3 transcription. However, this model has not been directly tested. Therefore, we integrated genetic, pharmacological, and epigenetic approaches to examine the function and mechanism of DNA demethylation in $T_{reg}$ lineage maintenance. We observed an abrupt switch of the transcriptional drivers of Foxp3 upon DNA demethylation, which was abolished by CNS2 deficiency. Demethylation of CNS2 increased chromatin accessibility and protein binding, conferring on $T_{reg}$ fate substantial resistance to adverse environments. Thus, our study consolidated the role of DNA demethylation in stabilizing Foxp3 expression in *cis* and revealed a novel regulatory mode governing $T_{reg}$ identity.

## INTRODUCTION

$T_{reg}$ cells are induced from precursor cells by cognate antigens in the presence of favorable environmental cues, including IL-2 and TGF-β, to suppress specific pathogenic T cells and maintain immune homeostasis (Josefowicz, Lu, & Rudensky, 2012; Savage, Klawon, & Miller, 2020). Successful $T_{reg}$ lineage commitment further relies on subsequent mechanisms to "lock in" the $T_{reg}$ fate (Fu et al., 2012; Yue, Lio, Samaniego-Castruita, Li, & Rao, 2019; Yue et al., 2016). Genetic fate mapping and acute depletion experiments indicate that $T_{reg}$ cells are long-lived and that their continuous activity is required to maintain immune tolerance (J. M. Kim, Rasmussen, & Rudensky, 2007; Rubtsov et al., 2010). Thus, a stable lineage in the absence of guidance cues or in the presence of adverse environments is critical for sustained $T_{reg}$ immune suppressive function.

41 $T_{reg}$ lineage commitment and function relies on nuclear factor Foxp3 (Brunkow et al., 2001;
42 Fontenot, Gavin, & Rudensky, 2003; M. Gavin & Rudensky, 2003; Hori, Nomura, & Sakaguchi, 2003;
43 Liston et al., 2007). Investigation of the mechanisms controlling Foxp3 expression has produced
44 enormous insights into $T_{reg}$ biology (Josefowicz et al., 2012; Sakaguchi et al., 2020; Savage et al.,
45 2020). Although a growing list of cell-extrinsic and -intrinsic factors was known to maintain $T_{reg}$ fate, an
46 epigenetic memory conferred by DNA demethylation was proposed as a key mechanism stabilizing
47 Foxp3 transcription (Polansky et al., 2008). This process is initiated by Tet dioxygenases and
48 accomplished by a multi-step enzymatic reaction. In the absence of *Tet2* and *Tet3*, $T_{reg}$ cells fail to
49 sustain Foxp3 expression (Nakatsukasa et al., 2019; Yue et al., 2019; Yue et al., 2016). Because
50 *Foxp3* enhancer CNS2 is demethylated by Tet enzymes in $T_{reg}$ cells and not in precursors or
51 conventional T cells (Polansky et al., 2008; Yue et al., 2016) and CNS2-deficiency leads to unstable
52 Foxp3 expression (Feng et al., 2014; X. Li, Liang, LeBlanc, Benner, & Zheng, 2014; Zheng et al.,
53 2010), Tet-dependent DNA demethylation was proposed to stabilize Foxp3 transcription through CNS2.

54 However, Tet enzymes also control the expression of many other genes (Nakatsukasa et al.,
55 2019; Ohkura et al., 2012; Yue et al., 2019), which may stabilize Foxp3 expression in *trans*. It is unclear
56 to what extent Tet-dependent *cis* and *trans* mechanisms contribute to the stability of Foxp3
57 transcription. A direct test of the sufficiency of CNS2 in mediating Tet-dependent stabilization of Foxp3
58 expression is lacking. Although several factors have been shown to maintain Foxp3 expression,
59 including IL-2/Stat5 signaling, Runx-CBFβ, Foxp1, Foxo1/Foxo3, and Akt/Pten (Feng et al., 2014;
60 Ghosh, Roy-Chowdhuri, Kang, Im, & Rudra, 2018; Ouyang et al., 2010; Rudra et al., 2009; Shrestha et
61 al., 2015), their relationships with Tet/DNA demethylation have not been fully explored. Addressing
62 these issues will produce important insights into the mechanisms governing $T_{reg}$ lineage stability critical
63 in various immunological settings.

64 Here, we modeled $T_{reg}$ lineage commitment and maintenance *ex vivo* with mouse primary T
65 cells by taking advantage of vitamin C (or ascorbic acid, ASC)–dependent Tet enzymatic activity

66 (Sasidharan Nair, Song, & Oh, 2016; Yue et al., 2016). We integrated pharmacological, genetic, and
67 epigenetic approaches to assess the role and underlying mechanisms of Tet-dependent DNA
68 demethylation in maintaining qualitative Foxp3 expression in *cis* through enhancer CNS2. Our study
69 uncovered a novel regulatory mode established by hypomethylated CNS2, which switches the
70 transcriptional drivers of Foxp3 expression to maintain $T_{reg}$ identity.

71

72 **RESULTS**

73 **Histone acetylation drives both Foxp3 induction efficiency and expression levels during early**
74 **$T_{reg}$ cell development**

75 We first sought to uncover the driving force of Foxp3 transcription during $T_{reg}$ cell development.
76 To this end, we reexamined permissive histone acetylation (e.g., H3K27ac) in Foxp3 induction because
77 of its essential role in promoting gene expression (Fujisawa & Filippakopoulos, 2017). H3K27ac is
78 deposited by histone acetyltransferases (HATs) and read by bromodomain (BRD)-containing proteins
79 (Fujisawa & Filippakopoulos, 2017). Using Cut&Run sequencing (Fig. 1*A*), which probes epigenetic
80 modifications in their native states with improved resolution (Skene & Henikoff, 2017), we confirmed a
81 broad H3K27ac modification around the *Foxp3* locus in *ex vivo*–isolated $T_{reg}$ ($nT_{reg}$) cells but not in CD4
82 naïve T (Tn) cells. We then used pharmacological inhibitors to examine the stage-specific roles of
83 histone acetylation during $T_{reg}$ cell differentiation ($iT_{reg}$) from CD4 Tn cells *in vitro*, which recapitulates
84 $T_{reg}$ cell development *in vivo* (Feng et al., 2015; Josefowicz et al., 2012; Rudensky, 2011; Yue et al.,
85 2019). Blockade of HAT p300/CBP with C646, I-CBP112, or SGC-CBP30 reduced Foxp3 induction
86 efficiency in a dose-dependent manner (Figs. 1*B* and S1*A*, *B*). To test whether BRD proteins are
87 required to transduce the histone acetylation signal, we treated differentiating T cells with BRD
88 inhibitors JQ1, I-BET151, bromosporine, or PFI-1, resulting in a dose-dependent inhibition of Foxp3
89 induction efficiency (Figs. 1*C* and S1*C*-*E*). These results confirmed the essential role of histone

90 acetylation signaling in driving Foxp3 induction during $T_{reg}$ cell development (Feng et al., 2015; Liu et
91 al., 2014).

92 Because $T_{reg}$ lineage determination is a qualitative trait and Foxp3 expression levels are a
93 quantitative one, we reasoned that these two categories of gene regulation could be controlled by
94 separate mechanisms. Therefore, we tested whether histone acetylation signaling plays different roles
95 in these two potentially distinct regulatory modes. In the presence of titrated amounts of HAT or BRD
96 inhibitors (e.g., JQ1), the relationship between Foxp3 induction efficiency and Foxp3 expression levels
97 demonstrated that qualitative and quantitative controls of Foxp3 expression were well correlated
98 ($R^2$=0.9975; Fig. 1*D*), suggesting that, at the early stage of $T_{reg}$ cell development, Foxp3 induction
99 efficiency and Foxp3 expression levels could be controlled by the same mechanisms. Because
100 blockade of HATs or BRD proteins suppresses global gene expression during T cell activation and
101 differentiation, thereby inhibiting Foxp3 expression, we then added JQ1 into culture media 2 days after
102 CD4 Tn cells being cultured in $T_{reg}$-induction conditions. This acute blockade of BRD proteins abruptly
103 reduced the number of Foxp3-expressing cells (Fig. 1*E*), and the remaining Foxp3$^+$ cells showed
104 significantly lower levels of Foxp3 and its target genes (e.g., CD25, GITR, and CTLA-4) (Fig. S1*F*).
105 These results indicate that histone acetylation signaling determines both Foxp3 induction efficiency and
106 expression levels during early $T_{reg}$ cell development.

107 **Tet enzymes switch the driving force of qualitative Foxp3 expression**

108 After stochastic induction, Foxp3 expression is maintained in differentiated $T_{reg}$ cells during their
109 long lifespan. Tet-dependent DNA demethylation was proposed to be the main mechanism acting in *cis*
110 to “lock in” Foxp3 expression in committed $T_{reg}$ cells. Yet, the nature of the transition from Foxp3
111 induction to maintenance remains unclear. Because this process is not readily accessible in $T_{reg}$ cell
112 differentiating *in vivo* (Fig. 2*A*), we modeled $T_{reg}$ lineage commitment *in vitro* using mouse CD4 Tn cells
113 in the presence or absence of Tet-induced DNA demethylation (Sasidharan Nair et al., 2016; Yue et al.,
114 2016).

115 We isolated CD4 Tn cells from wild-type (WT) *Foxp3*$^{gfp}$ knock-in mice and induced iT$_{reg}$ cells in
116 media supplemented with or without ASC. To assess the stability or qualitative regulation of Foxp3
117 expression, we sorted iT$_{reg}$ cells by GFP expression 4 days later and cultured them in media containing
118 recombinant IL-2, IL-2 neutralization antibodies (aIL-2), or JQ1, with or without TCR restimulation by
119 anti-CD3 and anti-CD28 antibodies (Fig. 2*B*). More than 80% of mock-treated iT$_{reg}$ cells lost Foxp3
120 expression after TCR restimulation and IL-2 deprivation, whereas more than 50% of cells maintained
121 Foxp3 expression in the presence of IL-2 or absence of TCR restimulation (Fig. 2*C*). Similar to stable
122 nT$_{reg}$ cells, more than 80% of ASC-treated iT$_{reg}$ cells remained Foxp3$^{+}$ regardless of the culture
123 conditions (Figs. 2*C* and S2*A*). Notably, Foxp3 expression levels were still controlled by IL-2 and TCR
124 signaling in ASC-treated iT$_{reg}$ cells. These results strongly suggest that, after ASC treatment, qualitative
125 and quantitative Foxp3 expression are controlled by distinct mechanisms. To understand the features
126 of Foxp3 transcription during this transition, we labeled nascent RNA with pulsed ethynyl uridine to
127 directly compare the transient transcriptional activity of Foxp3 in mock-treated iT$_{reg}$ cells to that in ASC-
128 treated iT$_{reg}$ cells. We found that Foxp3 transcription was immediately silenced upon IL-2 deprivation in
129 mock-treated iT$_{reg}$ cells but not in ASC-treated iT$_{reg}$ cells (Fig. 2*D*, *E*). Together, these results indicate
130 that ASC treatment induced a drastic change of the mechanism governing qualitative Foxp3
131 transcription (e.g., from IL-2–sensitive to IL-2–insensitive regulations).

132 Next, we examined the role of histone acetylation signaling in stable Foxp3 expression. We
133 sorted mock- and ASC-treated iT$_{reg}$ cells and cultured them in media containing titrated amounts of
134 JQ1, which abruptly silenced Foxp3 expression in mock-treated iT$_{reg}$ cells (Fig. 2*F*). In contrast, Foxp3
135 expression was maintained in more than 85% of ASC-pretreated iT$_{reg}$ cells. Akin to IL-2 deprivation,
136 JQ1 reduced Foxp3 median fluorescence intensity (MFI) in both mock- and ASC-pretreated iT$_{reg}$ cells
137 (Fig. 2*G*). These data further indicate a profound transcriptional reprogramming of the qualitative
138 regulation of Foxp3 expression after ASC treatment.

139 To test whether Tet enzymes mediate the effect of ASC, we acutely ablated *Tet1*, *Tet2*, and

140 *Tet3* (*Tet1-3*) in CD4 Tn cells isolated from *Tet1-3*$^{fl/fl}$ mice with Cre-expressing retrovirus (Fig. 2*H*).
141 Because of the short time window of cell culture, our approach did not completely deplete Tet proteins
142 (Fig. S2*B*). Nonetheless, Cre-transduced $iT_{reg}$ cells significantly decreased the stability of Foxp3
143 expression in ASC-pretreated $iT_{reg}$ cells after being exposed to JQ1 or upon IL-2 neutralization (Fig. 2*I*).
144 Ablation of Tet proteins also reduced ASC-dependent upregulation of Foxp3 expression (Fig. 2*J*).
145 Neither ASC treatment nor Tet deficiency influenced Foxp3 induction efficiency (Fig. S2*C*). Histone
146 acetylation signaling and Tet activity coordinated to upregulate Foxp3 and CD25 expression levels in
147 $iT_{reg}$ cells (Figs. 2*J* and S2*D*). The latter may contribute to Tet/ASC–dependent stabilization of Foxp3
148 expression in *tran*s. Our results are consistent with the reported function of ASC in maintaining $T_{reg}$
149 identity through Tet enzymes (Sasidharan Nair et al., 2016; Yue et al., 2016). Importantly, we observed
150 that Tet enzymes drastically switched the drivers of qualitative Foxp3 transcription, conferring stable
151 $T_{reg}$ identity in adverse environments.

152 **Tet enzymes stabilize qualitative Foxp3 expression via enhancer CNS2**

153 Next, we examined the requirement for CNS2 in ASC-dependent stabilization of Foxp3
154 expression (Fig. 3*A*). We first performed whole-genome bisulfite sequencing (WGBS) to fine-map the
155 differential DNA methylation patterns in CD4 Tn, effector T (Te), $nT_{reg}$, and $iT_{reg}$ cells developed with or
156 without supplemented ASC. Because the *Foxp3* gene is on the X chromosome that undergoes random
157 inactivation, cells used for WGBS were isolated from male *Foxp3*$^{gfp}$ mice. Although global DNA
158 methylation ratios were not drastically different (Fig. S3*A*), differentially methylated regions (DMRs)
159 unambiguously distinguished these cell types, as illustrated by the principal component analysis (Fig.
160 S3*B*). Compared to CD4 Tn and Te cells, $nT_{reg}$ cells were hypomethylated at the *Foxp3* promoter,
161 CNS2, and several other regions in the locus (Fig. 3*B*). ASC treatment induced hypomethylation of
162 these DMRs in $iT_{reg}$ cells to a level comparable to that in $nT_{reg}$ cells despite reduced widths. Notably,
163 many $T_{reg}$-specific DMRs, such as *Lrrc32*, *Emsy*, *Il2ra*, *Ift80*, *Wdr82*, and *Ctla4*, were less
164 hypomethylated in ASC-treated $iT_{reg}$ cells (Fig. S4*A*). Although the cause of these differences was

165 unknown, our results (Figs. 3*B* and S4*B*-*G*) together with published reports (Sasidharan Nair et al.,
166 2016; Yue et al., 2016) indicate that ASC-treated $iT_{reg}$ cells serve as an excellent *ex vivo* model in
167 which to study the mechanistic processes of DNA demethylation–dependent control of Foxp3
168 transcription during $T_{reg}$ lineage commitment.

169 We then tested whether ASC-induced hypomethylation of CNS2 was indeed Tet-dependent. To
170 this end, we acutely ablated *Tet1-3* with retroviral Cre during $T_{reg}$ cell development, which abolished the
171 effect of ASC on CNS2 demethylation (Fig. 3*C*), consistent with the reported role of Tet/ASC in CNS2
172 demethylation (Sasidharan Nair et al., 2016; Yue et al., 2016). To uncover the global effect of ASC
173 treatment, we performed RNA-seq with mock- and ASC-treated $iT_{reg}$ cells, revealing 514 genes that
174 were up- or down-regulated ($p$<0.01 and fold change [FC] >2; Fig. 3*D*). Although these genes' exact
175 functions remain to be determined, this result suggests potential *trans* mechanisms controlling the
176 stability of Foxp3 expression.

177 To test this possibility, we assessed whether CNS2 was indeed responsible for Tet/ASC-
178 dependent stabilization of Foxp3 expression. We induced $iT_{reg}$ cells from CNS2-sufficient and -deficient
179 CD4 Tn cells in media supplemented with or without ASC. We then sorted $iT_{reg}$ cells after induction and
180 examined the stability of Foxp3 expression in adverse environments, including IL-4, IL-6, or JQ1, in the
181 presence of titrated amounts of TCR agonists. In mock-treated $iT_{reg}$ cells, TCR restimulation alone or in
182 combination with JQ1, IL-4, or IL-6 drastically diminished the percentages of Foxp3-expressing cells in
183 both CNS2-sufficient and -deficient cells (Fig. 3*E*-H). Notably, mock-treated CNS2-deficient $iT_{reg}$ cells
184 appeared to be less stable in Foxp3 expression than CNS2-sufficient $iT_{reg}$ cells, suggesting that CNS2
185 may also play a role in maintaining Foxp3 expression before DNA demethylation. In contrast, ASC
186 treatment drastically stabilized Foxp3 expression in WT $iT_{reg}$ cells regardless of the adverse
187 environments. The same treatment failed to stabilize Foxp3 expression in CNS2-deficient $iT_{reg}$ cells,
188 indicating that CNS2 is required for ASC-dependent stabilization of qualitative Foxp3 expression. As
189 CNS2's main function was enabled by ASC-treatment that relied on Tet enzymes, our results

190 demonstrated the sufficiency of Tet-induced DNA demethylation of CNS2 in stabilizing Foxp3
191 expression and excluded the significance of potential Tet/ASC-mediated *trans* mechanisms in
192 stabilizing Foxp3 expression. Our experiments also uncovered a novel regulatory mode established by
193 hypomethylated CNS2, predominantly switching the transcriptional driving force of qualitative Foxp3
194 expression to stabilize $T_{reg}$ lineage identity.

195 **DNA methylation controls chromatin accessibility and nuclear factor binding at CNS2**

196 To reveal the nature of this epigenetic mechanism, we first compared chromatin accessibility
197 with ATAC-seq (Buenrostro, Giresi, Zaba, Chang, & Greenleaf, 2013) among CD4 Tn, Te, $nT_{reg}$, and
198 mock- and ASC-treated $iT_{reg}$ cells. This experiment unbiasedly revealed significant differences between
199 the chromatin accessibility of mock-treated $iT_{reg}$ cells and that of ASC-treated $iT_{reg}$ cells (Fig. 4*A*, *B*). At
200 the *Foxp3* locus, we observed $T_{reg}$-specific accessible chromatin at CNS2, in agreement with a
201 published report (Samstein et al., 2012). Despite active Foxp3 transcription, CNS2 chromatin remained
202 inaccessible in mock-treated $iT_{reg}$ cells. Upon ASC treatment, CNS2 became accessible, suggesting
203 that DNA demethylation drastically remodels CNS2 chromatin architecture.

204 Increased chromatin accessibility of CNS2 may facilitate nuclear factor binding, thus rewiring
205 the regulatory circuits controlling Foxp3 transcription. To test this possibility, we assessed Stat5 binding
206 at CNS2 before and after DNA demethylation because of the reported roles of IL-2/Stat5 signaling in
207 $T_{reg}$ cell induction and lineage stability (Chinen et al., 2016; Fan et al., 2018; Feng et al., 2014). Stat5
208 ChIP-seq revealed 3,286 Stat5-binding sites, among which 164 showed significantly different ($p<0.05$)
209 intensities between mock- and ASC-treated $iT_{reg}$ cells (Fig. 4*C*). Stat5 binding at CNS2 in mock-treated
210 $iT_{reg}$ cells was barely noticeable, and ASC treatment increased Stat5 binding at CNS2 to a level
211 comparable to that in $nT_{reg}$ cells (Fig. 4*D*), indicating a causal role of DNA demethylation. In
212 comparison, Stat5 binding at enhancer CNS4 was independent of ASC treatment. Similar to CNS2,
213 ASC treatment induced DNA demethylation, open chromatin, and enhanced Stat5 binding at many
214 other regions (e.g., *Fam134b* and *Ldlrad4*) (Fig. S5*A*, *B*). In some cases, ASC treatment resulted in

215 DNA hypomethylation and increased Stat5 binding without changing chromatin accessibility (Fig. S5*C*-
216 *F*). Despite these differences, our data demonstrated an epigenetic switch induced by Tet/ASC–
217 induced DNA demethylation that controls Stat5 binding.

218 To test whether increased Stat5 binding at CNS2 was $T_{reg}$ cell–specific, we used ChIP-qPCR to
219 assess Stat5 binding at *Foxp3 cis*-regulatory elements in mock- and ASC-treated Th0 (activated CD4
220 Tn cells in neutral conditions) and $iT_{reg}$ cells. We observed Stat5 binding at CNS2 in ASC-treated $iT_{reg}$
221 cells but not in mock-treated $iT_{reg}$ cells or ASC-treated Th0 cells (Fig. 4*E*), in agreement with chromatin
222 accessibility of CNS2 in ASC-treated $iT_{reg}$ cells. To test whether Stat5 binding at CNS2 in ASC-treated
223 $iT_{reg}$ cells depends on Tet enzymes, we used retroviral Cre to acutely ablate *Tet1-3* in differentiating
224 $iT_{reg}$ cells two days before ASC treatment. This led to an abrupt reduction of Stat5 binding at CNS2
225 (Fig. 4*F*), confirming that the effect of ASC was achieved via Tet enzymes. Although the transition of
226 Tet/ASC–induced DNA demethylation cannot be readily captured during $T_{reg}$ cell development *in vivo*,
227 Stat5 binding was highly enriched at hypomethylated, accessible chromatin regions in $nT_{reg}$ cells (Fig.
228 4*G*, *H*), suggesting that DNA methylation controls chromatin accessibility and Stat5 binding, probably
229 as a general mechanism.

230 DNA methylation may also control the binding of other nuclear factors at CNS2. To test this
231 notion, we examined Foxp3 association with CNS2, a feedforward mechanism proposed to stabilize
232 $T_{reg}$ fate (Maruyama, Konkel, Zamarron, & Chen, 2011; Rudensky, 2011; Samstein et al., 2012).
233 Indeed, we observed increased Foxp3 binding at CNS2 in ASC-treated *Tet1-3*$^{fl/fl}$ $iT_{reg}$ cells, which was
234 diminished when cells were transduced with Cre-expressing retrovirus before their differentiation (Fig.
235 4*I*). Although the factors that differentially bind at hypomethylated CNS2 remain to be fully determined,
236 DNA demethylation appears to reprogram the regulatory circuits via CNS2 to stabilize Foxp3
237 transcription by modulating the binding of nuclear factors.

238 **DNA demethylation stabilizes qualitative Foxp3 transcription *in vitro* in the absence of Foxp3**
239 **feedforward regulation**

240 To reveal the roles of the regulatory circuits assembled via hypomethylated CNS2, we first
241 assessed the contribution of IL-2/Stat5 signaling. Surprisingly, enhanced Stat5 binding at CNS2
242 appeared to not account for stable, qualitative Foxp3 expression in ASC-treated $iT_{reg}$ cells, shown by
243 the percentage of $Foxp3^{+}$ cells after IL-2 deprivation (Fig. 2*C*). Consistently, low levels of IL-2 executed
244 only a subtle effect on the stability of Foxp3 expression in WT $nT_{reg}$ cells (Feng et al., 2014). Compared
245 with the hyper instability of Foxp3 expression in *Tet2/Tet3*–deficient or mock-treated $iT_{reg}$ cells, these
246 results suggest a possibility that other factors bound at hypomethylated CNS2 might play a major role.

247 Next, we tested whether Foxp3 binding at hypomethylated CNS2 provides a strong feedforward
248 mechanism to stabilize Foxp3 transcription, as similar circuits are widely used in cell fate determination
249 (Urban & Johnston, 2018). To this end, we used $Foxp3^{loxP\text{-}Thy1.1\text{-}Stop\text{-}loxP\text{-}gfp}$ ($Foxp3^{LSL}$) knock-in mice (Hu
250 et al, submitted) to report Foxp3 transcription by Thy1.1 expression without producing functional Foxp3
251 protein, thus they are comparable to $Foxp3^{null}$ or scurfy mice (Fig. 5*A*). Because these mice have very
252 few CD4 Tn cells as a result of severe immune activation, we generated chimeric mice with WT CD45.1
253 and $Foxp3^{LSL}$ CD45.2 bone marrows mixed at a 1:1 ratio to suppress autoreactive conventional T cells
254 (Fig. 5*B*). We isolated $Foxp3^{LSL}$ CD4 Tn cells (CD45.2) from these healthy chimeric mice and induced
255 Thy1.1-expressing "wannabe" $iT_{reg}$ cells in $T_{reg}$-induction conditions with or without supplemented ASC.
256 We then sorted $Thy1.1^{+}$ cells after induction to assess the stability of Thy1.1 expression in media
257 containing JQ1, recombinant IL-2, or IL-2 neutralization antibodies.

258 Lack of Foxp3 protein expression appeared to be dispensable for Thy1.1 induction efficiency
259 (Fig. 5*C*), indicating that Foxp3 feedforward regulation plays a minor role in $T_{reg}$ cell development. ASC
260 treatment led to a mild increase of GFP-Foxp3 fusion protein in $iT_{reg}$ cells and of Thy1.1 protein in
261 wannabe $iT_{reg}$ cells (Fig. 5*D*). In $T_{reg}$ *in vitro* stability assay, more than 55% of control $iT_{reg}$ cells and
262 more than 80% of wannabe $iT_{reg}$ cells failed to maintain Foxp3 or Thy1.1 expression, respectively, with
263 the latter showing a significantly more instability (Fig. 5*E*). This result indicates that Foxp3 feedforward
264 loop plays a role in sustaining Foxp3 transcription before Tet/ASC–induced DNA demethylation. After

265 ASC treatment, however, lack of Foxp3 feedforward regulation did not affect the stability of Thy1.1
266 expression in the presence of JQ1 or upon IL-2 deprivation. As CNS2 is required for Tet/ASC–
267 dependent stabilization of Foxp3 transcription, these data indicate that Stat5 and Foxp3 binding at
268 hypomethylated CNS2 is insufficient to account for the drastically increased stability of Foxp3
269 transcription upon Tet/ASC–induced DNA demethylation.

270 **Foxp3 feedforward loop and maintenance of Foxp3 transcription and $T_{reg}$ cell fitness *in vivo***

271 We then examined the roles of the Foxp3 feedforward loop *in vivo*. We sorted Thy1.1$^+$ wannabe
272 $iT_{reg}$ cells after induction and cotransferred them with CD45.1 Tn and $nT_{reg}$ cells into *Rag1*$^{-/-}$ mice (Fig.
273 6*A*). Two weeks later, approximately 20% of control and 80% of ASC-pretreated wannabe $iT_{reg}$ cells
274 maintained Thy1.1 expression (Fig. 6*B*, *C*), further confirming that Tet-induced DNA demethylation
275 stabilizes qualitative Foxp3 transcription in the absence of the Foxp3 feedforward loop. To test whether
276 Foxp3 transcription can be stably maintained in the presence or absence of Foxp3 protein in $nT_{reg}$ and
277 wannabe $T_{reg}$ cells developed *in vivo*, we sorted GFP$^+$ CD4 T cells from male *Foxp3*$^{gfp}$ mice and
278 Thy1.1$^+$ CD4 T cells from male *Foxp3*$^{LSL}$ mice and co-transferred them with CD45.1 CD4 Tn and $nT_{reg}$
279 cells into *Rag1*$^{-/-}$ mice (Fig. 6*D*). Two weeks later, approximately 90% of $nT_{reg}$ cells maintained Foxp3
280 expression and 70-80% of wannabe $T_{reg}$ cells remained Thy1.1$^+$ (Fig. 6*E*). The latter rate was
281 comparable to that of ASC-pretreated wannabe $iT_{reg}$ cells (Fig. 6*C*). Taken together, these results
282 indicate that Foxp3 feedforward regulation is a minor contributor to Tet-induced stable qualitative Foxp3
283 transcription.

284 Despite comparable stability of qualitative Foxp3 transcription, absence of Foxp3 protein
285 reduced CD25 and CTLA-4 expression in a cell intrinsic manner (Fig. 6*F*, *G*), consistent with the
286 reported function of Foxp3 (Fontenot et al., 2003; M. A. Gavin et al., 2007; Hori et al., 2003). Because
287 CD25 confers on IL-2 receptors an approximately 100-fold higher affinity to IL-2 (Malek & Castro, 2010)
288 and IL-2 signaling plays a critical role in $T_{reg}$ cell survival and fitness, lower levels of CD25 may
289 contribute to the decrease in wannabe $T_{reg}$ cell numbers (Fig. 6*H*). Thus, Stat5 and Foxp3 binding at

290 hypomethylated CNS2 may play only a minor role in stabilizing qualitative Foxp3 transcription after Tet-
291 induced DNA demethylation (Fig. 6*l*). Our data suggest that other factors and mechanisms may
292 contribute to the abrupt switch of the driving force that stabilizes qualitative Foxp3 transcription upon
293 Tet-dependent DNA demethylation during $T_{reg}$ cell development.

294

295 **DISCUSSION**

296 We aim to uncover the nature of qualitative and quantitative regulations of Foxp3 transcription
297 during the transition from $T_{reg}$ cell induction to lineage maintenance. Tet enzymes were proposed to
298 stabilize qualitative Foxp3 transcription in *cis* by demethylating the *Foxp3* enhancer CNS2. However,
299 this model has not been directly tested, leaving its real role and underlying mechanisms uncertain.
300 Given the potential global effect of Tet-dependent DNA demethylation, it is unclear whether and to what
301 extent Tet enzymes stabilize Foxp3 expression through CNS2. Besides observed DNA
302 hypomethylation of CNS2 in $T_{reg}$ cells and impaired stability of qualitative Foxp3 expression in Tet- or
303 CNS2-deficient $T_{reg}$ cells (Sakaguchi et al., 2020), how DNA demethylation stabilizes Foxp3 expression
304 in its native genomic context is also unclear.

305 As no markers are available to readily distinguish the developmental stages of $T_{reg}$ cells *in vivo*,
306 we modeled $T_{reg}$ lineage commitment using *ex vivo*–isolated mouse T cells. Limited ASC in regular
307 culture medium enables us to control Tet enzymatic activity via supplemented ASC (Sasidharan Nair et
308 al., 2016; Yue et al., 2016). This treatment reliably demethylates *Foxp3 cis*-regulatory elements and
309 stabilizes qualitative Foxp3 transcription in $iT_{reg}$ cells, recapitulating the key features of $T_{reg}$ lineage
310 commitment (Rudensky, 2011; Sakaguchi et al., 2020). Using this model, we directly assessed the role
311 of Tet-dependent DNA demethylation in stabilizing Foxp3 expression, thereby affecting $T_{reg}$ lineage
312 identity in *cis* via enhancer CNS2. ASC-treated $iT_{reg}$ cells and $nT_{reg}$ cells share similar DNA methylation
313 levels, chromatin accessibility, and Foxp3 and Stat5 binding at CNS2. However, $nT_{reg}$ and ASC-treated

314 $iT_{reg}$ cells are not identical in DNA methylation patterns, indicating considerable differences in Tet
315 recruitment and/or enzymatic activity. Nonetheless, ASC treatment stabilizes Foxp3 transcription in $iT_{reg}$
316 cells in a CNS2-dependent manner, demonstrating the essential role of the Tet/ASC-CNS2 axis in
317 sustaining qualitative Foxp3 expression and $T_{reg}$ lineage identity. It also distinguishes the *cis* and *trans*
318 effects of Tet/ASC-mediated DNA demethylation on $T_{reg}$ lineage stability.

319 Tet/ASC–induced DNA demethylation increased the chromatin accessibility of CNS2,
320 accompanied by markedly enhanced Stat5 and Foxp3 binding. These observations provide a
321 mechanistic understanding of how DNA methylation controls the stage-specific activity of CNS2.
322 Although similar phenomena have been shown by *in vitro* binding and reporter assays (H. P. Kim &
323 Leonard, 2007; Polansky et al., 2010; Zheng et al., 2010), in the absence of native genomic context,
324 such results did not reveal the exact function of the factors bound at hypomethylated CNS2. We found
325 that demethylation of CNS2 induces a drastic switch of the regulatory modes of Foxp3 transcription,
326 enabling stable, qualitative Foxp3 expression in adverse conditions while maintaining its quantitative
327 regulation by IL-2 and permissive histone acetylation signaling. Counterintuitively, however, enhanced
328 Stat5 binding at hypomethylated CNS2 appears to play only a minor role in stabilizing Foxp3
329 expression. Similarly, ASC treatment largely stabilizes Foxp3 transcription in the absence of the Foxp3
330 feedforward loop with or without IL-2 deprivation. Therefore, the real functions of the factors bound at
331 hypomethylated CNS2 should be examined experimentally in the native genomic context during $T_{reg}$
332 lineage maintenance.

333 Our study of Stat5 and Foxp3 binding raised the question of whether a single factor bound at
334 hypomethylated CNS2 accounts for the drastically enhanced stability of qualitative Foxp3 transcription.
335 Previous studies identified several factors bound at the *Foxp3 cis*-regulatory elements to maintain
336 Foxp3 expression, such as CBFβ (Rudra et al., 2009). However, it is unclear to what extent their roles
337 are mediated by CNS2's demethylation. The 12 CpG sites scattered in the CNS2 region undergo a
338 drastic demethylation during $T_{reg}$ lineage commitment in a Tet/ASC–dependent manner, suggesting that

339 DNA demethylation could control the binding of multiple nuclear factors at CNS2 (Fig. 6*I*). If each of
340 them contributes a part to CNS2's function, then CNS2 demethylation likely creates "parallel" regulatory
341 circuits to stabilize Foxp3 transcription, so loss of any individual factor's binding would not generate a
342 catastrophic effect. Therefore, $T_{reg}$ lineage identity could be maintained by these partially redundant
343 mechanisms to oppose the fluctuations of individual proteins caused by adverse environments or
344 genetic variations. In addition, particular proteins or keystone factors associated with hypomethylated
345 CNS2 alone may be essential for stable Foxp3 expression, and their single deficiency could severely
346 impair the stability of Foxp3 expression. These proteins may be the unique constituents of CNS2 or
347 indispensable components of enhanceosomes in general. Given the exceptional stability of $T_{reg}$ lineage
348 identity, the keystone factors are likely abundant in $T_{reg}$ cells, akin to housekeeping genes or generic
349 transcription factors, such that robust Foxp3 transcription can be sustained in the presence of various
350 perturbations. Therefore, identifying and characterizing the proteins associated with hypomethylated
351 CNS2 will produce important new insights into the mechanisms governing $T_{reg}$ lineage stability.

352 In summary, we modeled the processes of $T_{reg}$ lineage commitment with mouse primary T cells
353 to directly investigate the role and underlying mechanisms of Tet/ASC–induced DNA demethylation in
354 controlling qualitative Foxp3 transcription and, thereby, $T_{reg}$ lineage identity. Our results proved the
355 proposed model of Tet/ASC-CNS2 axis in sustaining Foxp3 expression, distinguished it from alternative
356 mechanisms, and uncovered an epigenetic switch of the driving force of qualitative Foxp3 expression
357 after Tet-dependent DNA demethylation during $T_{reg}$ cell development. Thus, our study consolidates the
358 basis for further investigation of the mechanisms controlling $T_{reg}$ lineage commitment and maintenance,
359 an essential step to fully understanding $T_{reg}$-mediated immune tolerance in various immunological
360 settings.

361 **ACKNOWLEDGMENTS AND FUNDING SOURCES**

362 We thank Alexander Rudensky for providing the mouse strains, the Hartwell Center for high-
363 throughput sequencing, the Flow Cytometry Core facility for assistance with cell sorting and analysis,

364 Jaeki Min and Zoran Rankovic for providing epigenetic inhibitors, Cherise Guess for editing the
365 manuscript, and Ruopeng Feng for help with the Cut&Run experiments. X.Z. was supported by an APO
366 Special Postdoctoral Fellowship of St. Jude Children's Research Hospital. This study was supported by
367 the American Lebanese Syrian Associated Charities and the NIH grant R21AI146614 (Y. Feng.). The
368 content is solely the responsibility of the authors and does not necessarily represent the official
369 views of the National Institutes of Health.

370 **AUTHOR CONTRIBUTIONS**

371 J.L. and Y. Feng. conceived of and designed the experiments and interpreted the results. X.Z.
372 quantified nascent Foxp3 mRNA and provided critical comments. M.H. performed the Cut&Run
373 experiments and interpreted the results. B.X. and Y. Fan analyzed the high-throughput sequencing
374 data. R.C. provided assistance with FACS sorting. J.H. provided *Tet1-3*$^{fl/fl}$ mice. J.L. and Y. Feng. wrote
375 the manuscript.

376 **CONTACT FOR REAGENT AND RESOURCE SHARING**

377 Further information and requests for resources and reagents should be directed to Yongqiang
378 Feng (yong.feng@stjude.org).

379 **DECLARATION OF INTEREST**

380 The authors declare no competing interests.

381 **FIGURE LEGENDS**

382 **Fig. 1. Histone acetylation drives both Foxp3 induction efficiency and expression levels during**
383 **early $T_{reg}$ cell development.**

384 (*A*) Quantification of histone H3K27ac modification around the *Foxp3* locus (mm9) in CD4 Tn and $nT_{reg}$
385 cells by Cut&Run-seq. Positions of the *Foxp3* promoter (Pro) and enhancers are highlighted. Cons,
386 DNA sequence conservation among placental mammals.

387 (*B*) Foxp3 induction efficiency in the presence of titrated C646 during $T_{reg}$ cell development *in vitro*. CD4
388 Tn cells were cultured in $T_{reg}$-induction conditions (TCR agonists, IL-2, and TGF-β) with or without C646
389 for 4 days before analyzing Foxp3 expression. Data depict means + SEMs of triplicates and represent 3
390 independent experiments.

391 (*C*, *D*) Foxp3 induction efficiency in the presence of titrated JQ1 during $T_{reg}$ cell development *in vitro*
392 (*C*). Correlation of Foxp3 induction efficiency and Foxp3 expression levels per cell (median
393 fluorescence intensity, MFI) was calculated (*D*). Data depict means + SEMs of triplicates and represent
394 3 experiments.

395 (*E*) Inhibition of BRD proteins silenced Foxp3 expression at the late stages of $T_{reg}$ cell development.
396 JQ1 (1 μM) was added after CD4 Tn cells were cultured in $T_{reg}$-induction media for 2 days. Foxp3
397 expression was analyzed on day 4. Data depict means + SEMs of triplicates and represent 2
398 independent experiments. ***$p<0.001$ (unpaired, two-tailed *t* test).

399 See also Fig. S1.

Figure 1

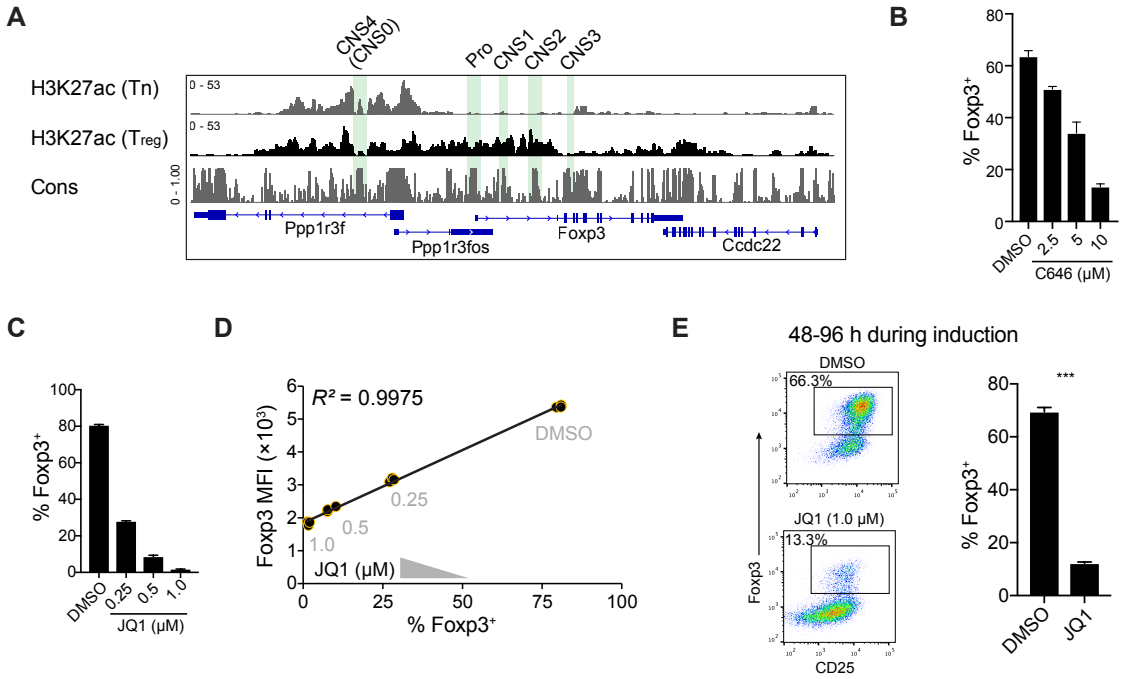
A
CNS4 (CNS0)
Pro
CNS1
CNS2
CNS3
H3K27ac (Tn)
H3K27ac (Treg)
Cons
0 - 53
0 - 53
0 - 1.00
Ppp1r3f
Ppp1r3fos
Foxp3
Ccdc22
B
% Foxp3+
DMSO
2.5
5
10
C646 (μM)
C
% Foxp3+
DMSO
0.25
0.5
1.0
JQ1 (μM)
D
R² = 0.9975
Foxp3 MFI (×10³)
% Foxp3+
DMSO
0.25
0.5
1.0
JQ1 (μM)
E
48-96 h during induction
DMSO
66.3%
JQ1 (1.0 μM)
13.3%
Foxp3
CD25
% Foxp3+
***
DMSO
JQ1

400 **Fig. 2. Tet enzymes switch the driving force of qualitative Foxp3 expression.**

401 (*A*) Schematic processes of $T_{reg}$ lineage commitment. Foxp3 expression is triggered by $T_{reg}$-induction
402 cues and stabilized by ASC-dependent Tet enzymatic activity. mCpG, methylated CpG. The off rate
403 indicates the instability of Foxp3 expression.

404 (*B*) Experimental procedures for assaying the stability of Foxp3 expression *in vitro*. On day 4, $iT_{reg}$ cells
405 induced with or without supplemented ASC were isolated and then grown in media containing
406 recombinant IL-2, IL-2 neutralization antibodies (aIL-2), or JQ1 with or without TCR restimulation for an
407 additional 4 days before analysis.

408 (*C*) Stability and levels of Foxp3 expression in mock- and ASC-pretreated (gray shaded) $iT_{reg}$ cells
409 grown in media containing recombinant IL-2 or aIL-2 with or without TCR restimulation by plate-bound
410 anti-CD3 and anti-CD28 antibodies. Dots indicate technical replicates. Data represent 2 experiments.

411 (*D*, *E*) Quantification of transient Foxp3 transcription. Mock- and ASC-treated $iT_{reg}$ cells were cultured
412 with IL-2 or aIL-2 for 20 h and then pulse-chased with ethynyl uridine (EU) for 45 min before
413 quantification of EU-labeled nascent Foxp3 mRNA via RT-qPCR. Signals of EU-enriched mRNA were
414 normalized to those of input cells in each sample. ****$p$<0.0001 (two-tailed, unpaired *t* test).

415 (*F*, *G*) Stability and levels of Foxp3 expression in mock- and ASC-pretreated $iT_{reg}$ cells grown in media
416 containing titrated JQ1 for an additional 4 days. Data represent more than 3 independent experiments.

417 (*H-J*) *Tet1-3*$^{fl/fl}$ CD4 Tn cells were cultured in $T_{reg}$-induction medium before being transduced with Cre-
418 expressing retrovirus on day 1. PBS or ASC was added from day 3 to day 5. Cells were then grown in
419 media containing DMSO (with IL-2), aIL-2, or JQ1 (with IL-2) with TCR restimulation for an additional 3
420 days before analysis. Data show means + SEMs of triplicates and represent one of 2 independent
421 experiments. ns, not significant; *$p$<0.05, **$p$<0.01, ****$p$<0.0001 (two-tailed, unpaired *t* test).

422 See also Fig. S2.

Figure 2

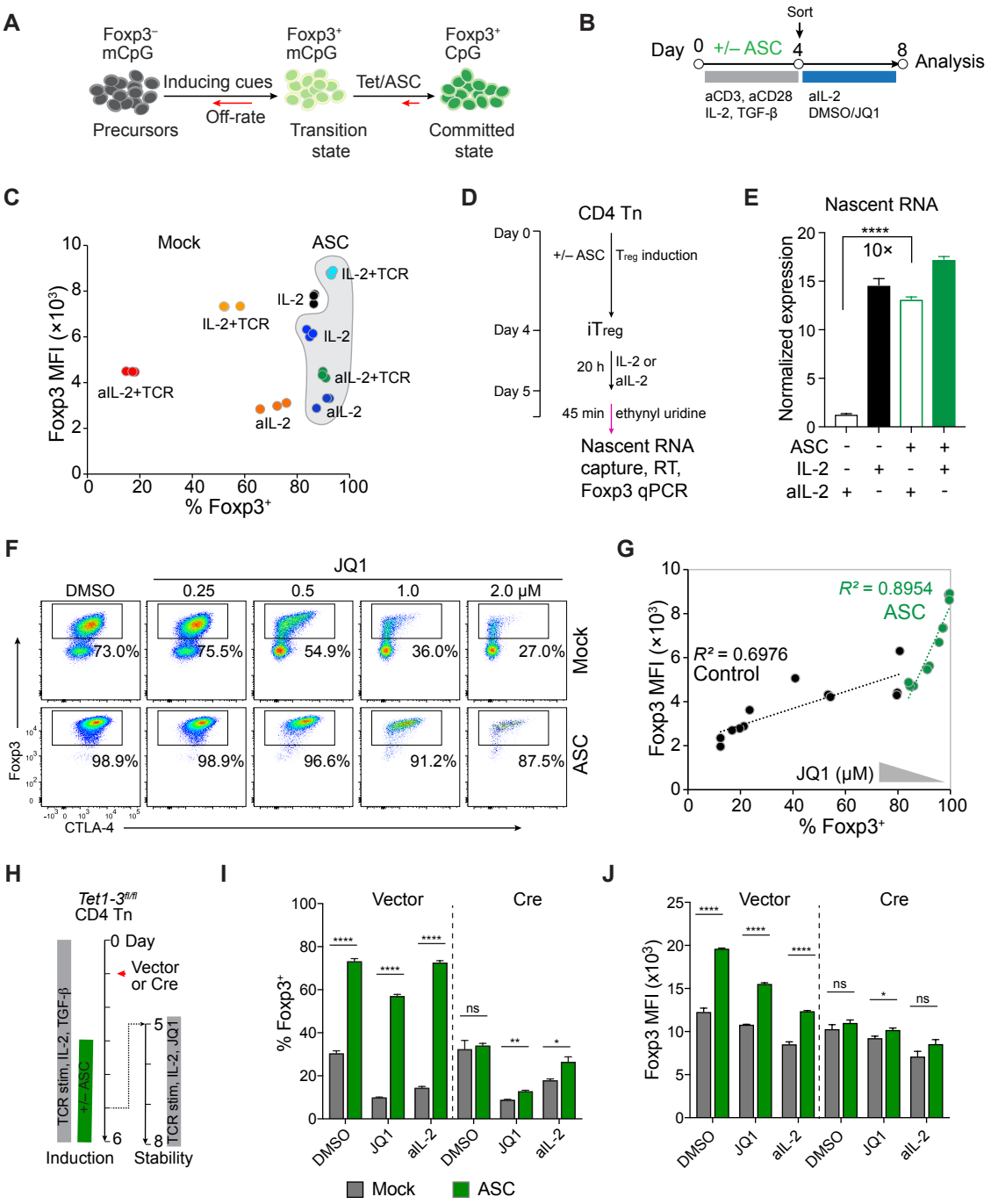
A
Foxp3⁻ mCpG
Foxp3⁺ mCpG
Foxp3⁺ CpG
Inducing cues
Off-rate
Tet/ASC
Precursors
Transition state
Committed state
B
Sort
Day 0 +/– ASC 4 8 Analysis
aCD3, aCD28
IL-2, TGF-β
aIL-2
DMSO/JQ1
C
Mock
ASC
IL-2+TCR
IL-2
aIL-2+TCR
aIL-2
Foxp3 MFI (×10³)
% Foxp3⁺
D
CD4 Tn
Day 0
+/– ASC
Treg induction
iTreg
Day 4
20 h
IL-2 or aIL-2
Day 5
45 min
ethynyl uridine
Nascent RNA capture, RT, Foxp3 qPCR
E
Nascent RNA
****
10×
Normalized expression
ASC
IL-2
aIL-2
F
JQ1
DMSO
0.25
0.5
1.0
2.0 μM
73.0%
75.5%
54.9%
36.0%
27.0%
Mock
98.9%
98.9%
96.6%
91.2%
87.5%
ASC
Foxp3
CTLA-4
G
R² = 0.8954
ASC
R² = 0.6976
Control
JQ1 (μM)
Foxp3 MFI (×10³)
% Foxp3⁺
H
Tet1-3fl/fl
CD4 Tn
0 Day
Vector or Cre
TCR stim, IL-2, TGF-β
+/– ASC
TCR stim, IL-2, JQ1
Induction
Stability
I
Vector
Cre
% Foxp3⁺
****
ns
**
*
DMSO
JQ1
aIL-2
Mock
ASC
J
Vector
Cre
Foxp3 MFI (x10³)
****
ns
*

423 **Fig. 3. Tet enzymes stabilize qualitative Foxp3 expression via enhancer CNS2.**

424 (*A*) Experimental procedures of assaying $T_{reg}$ stability, differential gene expression, and WGBS with
425 $iT_{reg}$ cells induced from *Foxp3*$^{gfp}$ CD4 Tn cells with or without supplemented ASC.

426 (*B*) DNA (CpG) methylation ratios around the *Foxp3* locus (mm9) in CD4 Tn cells, effector T (Te) cells,
427 $nT_{reg}$ cells, and mock- or ASC-treated $iT_{reg}$ cells. Vertical lines represent individual CpG sites and
428 methylation levels from 0 (unmethylated) to 1 (methylated). Data were merged from 2 biological
429 replicates. Regions covered by < 5 reads are marked as -0.2.

430 (*C*) Quantification of the methylation status at select CpG sites of CNS2 by bisulfite PCR-seq in $iT_{reg}$
431 cells after acute deletion of Tet enzymes followed by mock and ASC treatment. Rows of dots represent
432 individual DNA molecules.

433 (*D*) Genes that are differentially expressed in mock- and ASC-treated $iT_{reg}$ cells. Data were merged
434 from 2 biological replicates.

435 (*E-H*) Stability of Foxp3 expression in WT *Foxp3*$^{gfp}$ and *Foxp3*$^{\Delta CNS2\text{-}gfp}$ $iT_{reg}$ cells pretreated with or
436 without ASC. Cells were then restimulated with titrated amounts of plate-bound anti-CD3 antibody and
437 constant anti-CD28 antibody (1 μg/mL) in media containing recombinant IL-2 (100 U/mL) and either
438 DMSO (*E*), JQ1 (2 μM) (*F*), IL-4 (10 ng/mL) (*G*), or IL-6 (20 ng/mL) (*H*) for 4 days before analysis.
439 *$p$<0.05, **$p$<0.01, ***$p$<0.001, ****$p$<0.0001 (unpaired, two-tailed *t* test). Data show means + SEMs of
440 triplicates and represent 3 experiments.

441 See also Figs. S3 and S4.

Figure 3

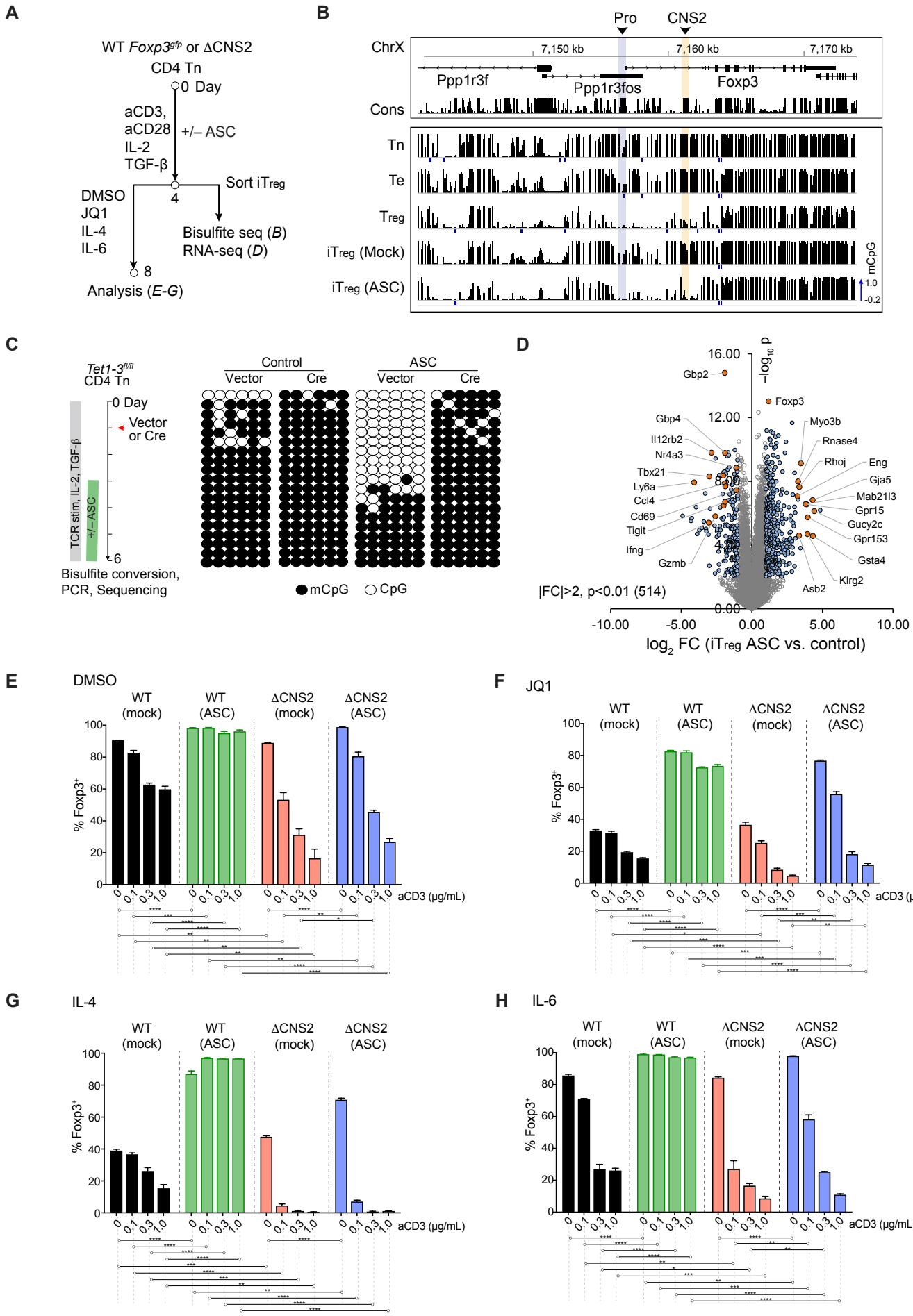
A
WT Foxp3gfp or ΔCNS2
CD4 Tn
0 Day
aCD3,
aCD28
IL-2
TGF-β
+/– ASC
Sort iTreg
DMSO
JQ1
IL-4
IL-6
4
Bisulfite seq (B)
RNA-seq (D)
8
Analysis (E-G)
B
Pro
CNS2
ChrX
7,150 kb
7,160 kb
7,170 kb
Ppp1r3f
Ppp1r3fos
Foxp3
Cons
Tn
Te
Treg
iTreg (Mock)
iTreg (ASC)
mCpG
1.0
-0.2
C
Tet1-3fl/fl
CD4 Tn
0 Day
Vector
or Cre
TCR stim, IL-2, TGF-β
+/– ASC
6
Bisulfite conversion,
PCR, Sequencing
Control
ASC
Vector
Cre
Vector
Cre
mCpG
CpG
D
−log10 p
16.00
12.00
8.00
4.00
0.00
Gbp2
Foxp3
Gbp4
Il12rb2
Nr4a3
Tbx21
Ly6a
Ccl4
Cd69
Tigit
Ifng
Gzmb
Myo3b
Rnase4
Rhoj
Eng
Gja5
Mab21l3
Gpr15
Gucy2c
Gpr153
Gsta4
Klrg2
Asb2
|FC|>2, p<0.01 (514)
-10.00
-5.00
0.00
5.00
10.00
log2 FC (iTreg ASC vs. control)
E
DMSO
WT (mock)
WT (ASC)
ΔCNS2 (mock)
ΔCNS2 (ASC)
% Foxp3+
aCD3 (μg/mL)
F
JQ1
G
IL-4
H
IL-6

442 **Fig. 4. DNA methylation controls chromatin accessibility and nuclear factor binding at CNS2.**

443 (*A*, *B*) Genome-wide differential chromatin accessibility of mock- and ASC-treated $iT_{reg}$ cells (*A*) and
444 local chromatin accessibility around the *Foxp3* locus in $nT_{reg}$ cells and in mock- and ASC-treated $iT_{reg}$
445 cells derived from male *Foxp3*$^{gfp}$ mice (*B*) assessed by ATAC-seq. Data represent >3 experiments.

446 (*C*, *D*) Genome-wide differential Stat5 binding in mock- and ASC-treated $iT_{reg}$ cells (*C*) and Stat5
447 binding sites around the *Foxp3* locus in $nT_{reg}$ cells and in mock- and ASC-treated $iT_{reg}$ cells (*D*). Cells
448 were starved in IL-2–free media for 3 h and then stimulated with IL-2 (500 U/mL) for 30 min before
449 being harvested for Stat5 ChIP-seq. Data represent 2 independent experiments.

450 (*E*) Stat5 ChIP-qPCR with mock- and ASC-treated $iT_{reg}$ and neutrally activated CD4 Tn cells (Th0 cells)
451 after 30 min of IL-2 stimulation. Data represent 2 independent experiments.

452 (*F*) Quantification of Stat5 binding at CNS2. *Tet1-3*$^{fl/fl}$ CD4 Tn cells were transduced with Cre-
453 expressing or control retrovirus 1 day after activation by TCR agonists and IL-2 in the presence or
454 absence of TGF-β (i.e., $iT_{reg}$ and Th0 culture conditions, respectively). ASC or PBS was added to media
455 on day 3. Then, 3-4 days later, transduced cells were sorted by Thy1.1 reporter expression for Stat5
456 ChIP-qPCR. Data show means + SEMs of triplicates and represent 2 experiments.

457 (*G*) Differential CpG methylation and chromatin accessibility of $nT_{reg}$ and CD4 Te cells. Dots represent
458 individual ATAC-seq peaks. Stat5-binding sites in $nT_{reg}$ cells are superimposed. Heatmap shows the
459 quantiles of Stat5 peak intensities. Data are merged from 2 replicates.

460 (*H*) Gene set enrichment analysis of the relationship between the top 500 Stat5-binding sites and the
461 differential DNA methylation of $nT_{reg}$ and Te cells. Genes related to the top 16 Stat5 peaks are listed on
462 the right.

463 (*I*) Quantification of Foxp3 binding at CNS2 with ChIP-qPCR. Ablation of *Tet1-3* and $iT_{reg}$ cell induction
464 were performed as described in (*F*).

465 See also Fig. S5.

Figure 4

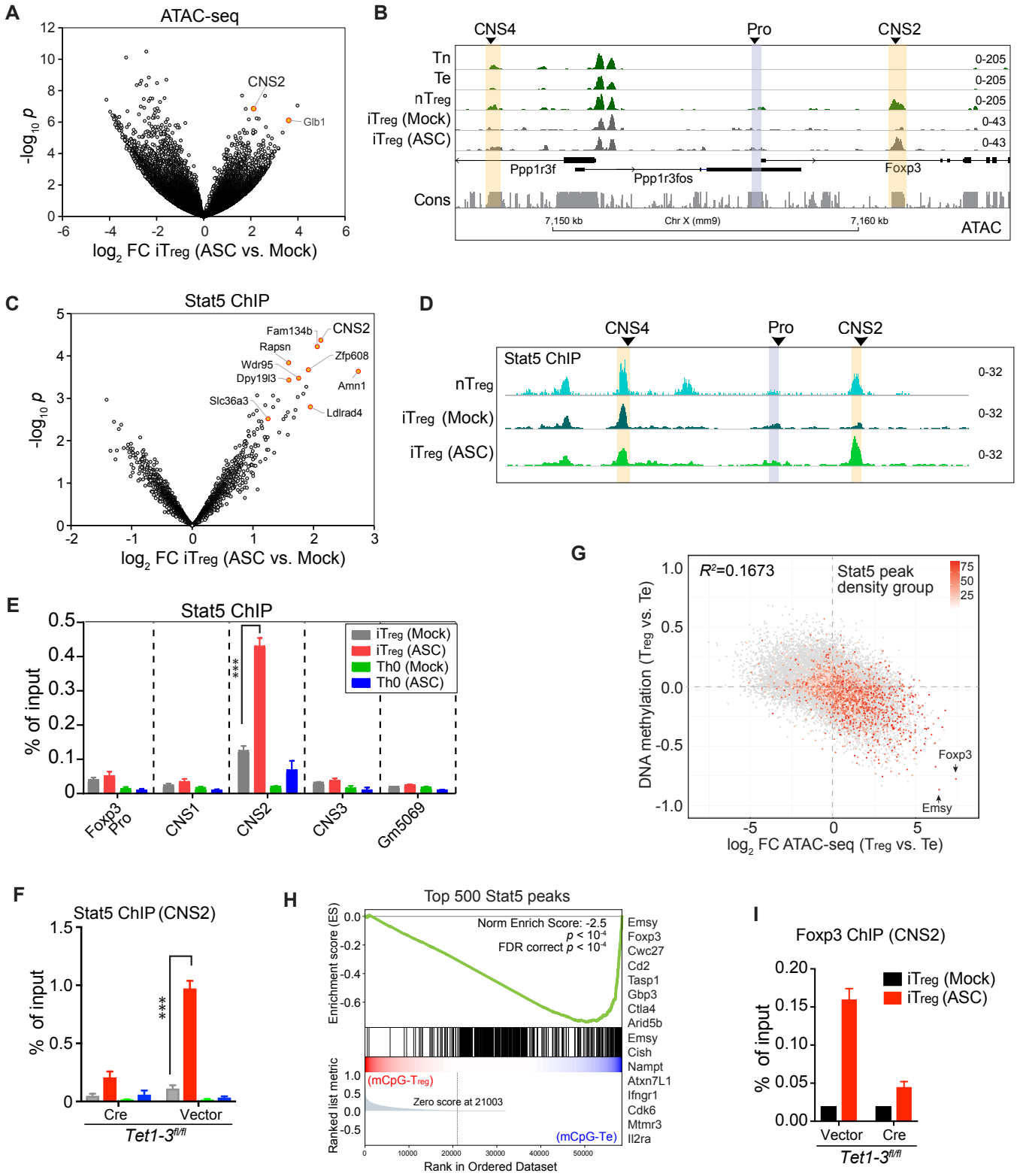
A
ATAC-seq
CNS2
Glb1
-log10 p
log2 FC iTreg (ASC vs. Mock)
B
CNS4
Pro
CNS2
Tn
Te
nTreg
iTreg (Mock)
iTreg (ASC)
0-205
0-43
Ppp1r3f
Ppp1r3fos
Foxp3
Cons
7,150 kb
Chr X (mm9)
7,160 kb
ATAC
C
Stat5 ChIP
Fam134b
CNS2
Rapsn
Zfp608
Wdr95
Dpy19l3
Amn1
Slc36a3
Ldlrad4
-log10 p
log2 FC iTreg (ASC vs. Mock)
D
CNS4
Pro
CNS2
Stat5 ChIP
nTreg
iTreg (Mock)
iTreg (ASC)
0-32
E
Stat5 ChIP
% of input
iTreg (Mock)
iTreg (ASC)
Th0 (Mock)
Th0 (ASC)
***
Foxp3 Pro
CNS1
CNS2
CNS3
Gm5069
G
R²=0.1673
Stat5 peak density group
75
50
25
DNA methylation (Treg vs. Te)
Foxp3
Emsy
log2 FC ATAC-seq (Treg vs. Te)
F
Stat5 ChIP (CNS2)
% of input
***
Cre
Vector
Tet1-3fl/fl
H
Top 500 Stat5 peaks
Norm Enrich Score: -2.5
p < 10-4
FDR correct p < 10-4
Enrichment score (ES)
Emsy
Foxp3
Cwc27
Cd2
Tasp1
Gbp3
Ctla4
Arid5b
Emsy
Cish
Nampt
Atxn7L1
Ifngr1
Cdk6
Mtmr3
Il2ra
Ranked list metric
(mCpG-Treg)
Zero score at 21003
(mCpG-Te)
Rank in Ordered Dataset
I
Foxp3 ChIP (CNS2)
iTreg (Mock)
iTreg (ASC)
% of input
Vector
Cre
Tet1-3fl/fl

466 **Fig. 5. DNA demethylation stabilizes qualitative Foxp3 transcription *in vitro* in the absence of**
467 **Foxp3 feedforward regulation.**

468 (*A*) Schematic of *Foxp3*$^{gfp}$ and *Foxp3*$^{LSL}$ knock-in mice. The latter reports Foxp3 transcription by Thy1.1
469 expression without producing Foxp3 protein in the absence of Cre recombinase.

470 (*B*) Experimental procedures of Thy1.1 induction and stability assays *in vitro*. Mixed bone marrow
471 chimeras of CD45.1 WT and CD45.2 *Foxp3*$^{LSL}$ mice were generated. Thy1.1-expressing wannabe $iT_{reg}$
472 cells were induced from *Foxp3*$^{LSL}$ CD4 Tn cells with or without ASC treatment. These cells were FACS-
473 sorted to assay the stability of Thy1.1 expression *in vitro*. Similarly, WT *Foxp3*$^{gfp}$ CD4 Tn cells were
474 used to examine the induction and stability of Foxp3 expression.

475 (*C*, *D*) Induction of Foxp3 and Thy1.1 expression from *Foxp3*$^{gfp}$ or *Foxp3*$^{LSL}$ CD4 Tn cells, respectively,
476 in the presence or absence of ASC. Data show means + SEMs of triplicates and represent 2
477 independent experiments. ** $p<0.01$, *** $p<0.001$ (unpaired, two-tailed *t* test).

478 (*E*) Stability of Foxp3 expression in mock- and ASC-pretreated $iT_{reg}$ cells and Thy1.1 expression in
479 wannabe $iT_{reg}$ cells. Sorted $GFP^+$ ($Foxp3^+$) or $Thy1.1^+$ cells were restimulated with TCR agonists in
480 media containing DMSO (100 U/mL IL-2), JQ1 (100 U/mL IL-2), IL-2 (100 U/mL; +IL-2), no recombinant
481 IL-2 (-IL-2), or aIL-2 (25 µg/mL) for 4 days before analysis. Data show means + SEMs of triplicates and
482 represent 2 independent experiments. * $p<0.05$, **** $p<0.0001$ (unpaired, two-tailed *t* test).

Figure 5

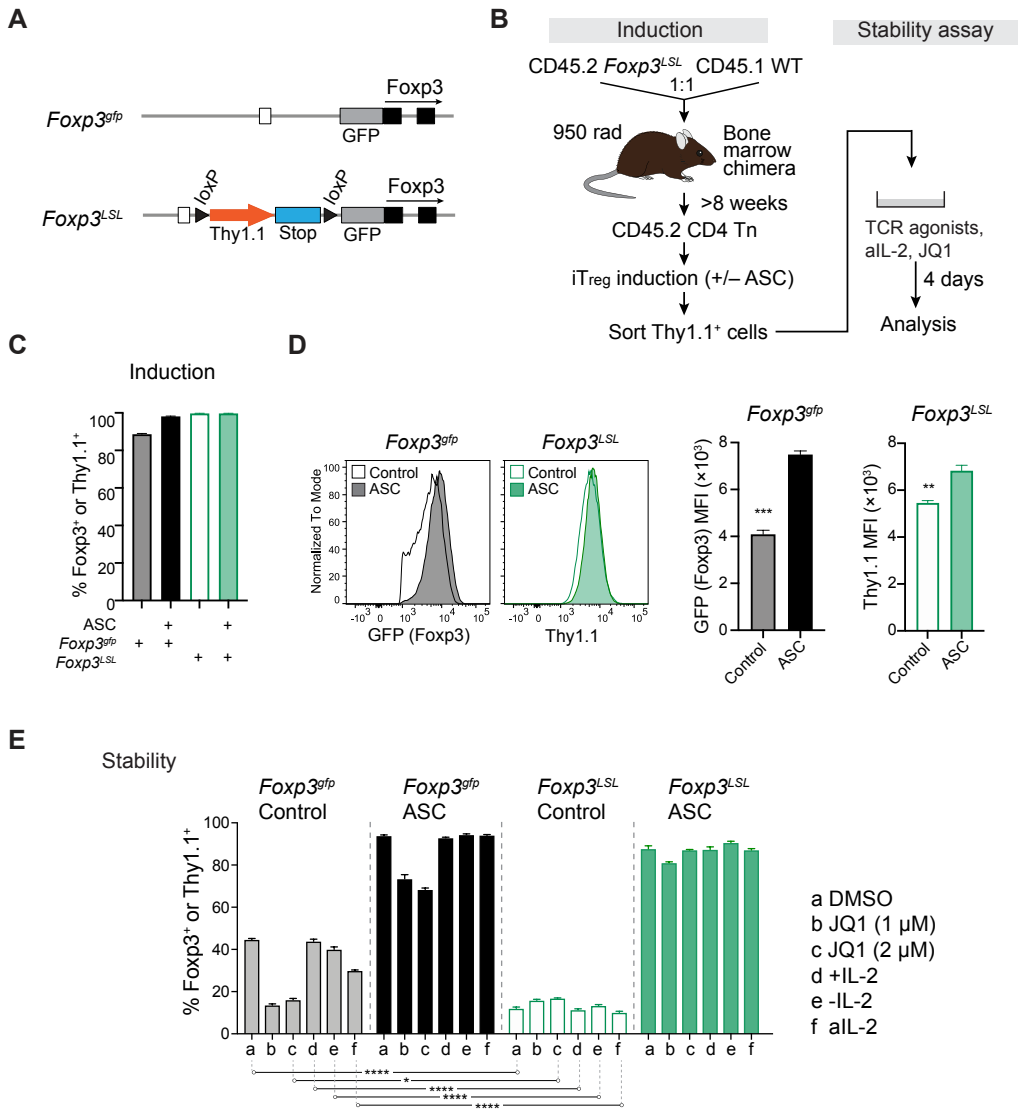
A
Foxp3gfp
Foxp3
GFP
Foxp3LSL
loxP
loxP
Foxp3
Thy1.1
Stop
GFP
B
Induction
Stability assay
CD45.2 Foxp3LSL
CD45.1 WT
1:1
950 rad
Bone marrow chimera
>8 weeks
CD45.2 CD4 Tn
iTreg induction (+/– ASC)
Sort Thy1.1+ cells
TCR agonists, aIL-2, JQ1
4 days
Analysis
C
Induction
% Foxp3+ or Thy1.1+
ASC
Foxp3gfp
Foxp3LSL
D
Foxp3gfp
Foxp3LSL
Control
ASC
Normalized To Mode
GFP (Foxp3)
Thy1.1
GFP (Foxp3) MFI (×10³)
Thy1.1 MFI (×10³)
Control
ASC
E
Stability
Foxp3gfp Control
Foxp3gfp ASC
Foxp3LSL Control
Foxp3LSL ASC
% Foxp3+ or Thy1.1+
a DMSO
b JQ1 (1 μM)
c JQ1 (2 μM)
d +IL-2
e -IL-2
f aIL-2

483 **Fig. 6. Roles of Foxp3 feedforward loop in maintaining Foxp3 transcription and $T_{reg}$ cell fitness**
484 ***in vivo*.**

485 (*A*) Experimental procedures for assessing the stability of Thy1.1 expression in wannabe $iT_{reg}$ cells *in*
486 *vivo*. CD4 Tn cells isolated from mixed bone marrow chimeric mice were used to induce Thy1.1
487 expression in $T_{reg}$-induction media with or without supplemented ASC. Thy1.1$^+$ cells were then sorted
488 and co-transferred with CD45.1 CD4 T cells (including $T_{reg}$ cells) into *Rag1*$^{-/-}$ recipient mice. Cells were
489 recovered 2 weeks later for analysis.

490 (*B-C*) Thy1.1 expression in recovered CD45.1$^-$CD4$^+$TCRβ$^+$ cells. n=5 each group. LN, lymph node;
491 MLN, mesenteric lymph node. *** $p$<0.01 (Mann-Whitney tests). Data represent 2 experiments.

492 (*D-H*) Stability of Foxp3 transcription in $nT_{reg}$ or wannabe $T_{reg}$ cells isolated from male *Foxp3*$^{gfp}$ or
493 *Foxp3*$^{LSL}$ mice. FACS-sorted CD4$^+$GFP$^+$ or CD4$^+$Thy1.1$^+$ cells were co-transferred with CD45.1 CD4 T
494 cells (including $T_{reg}$ cells) into *Rag1*$^{-/-}$ mice and recovered 2 weeks later to determine the percentages
495 of GFP$^+$ or Thy1.1$^+$ cells among CD45.1$^-$CD4$^+$TCRβ$^+$ cells (*E*). CD25 (*F*) and CTLA-4 (*G*) median
496 fluorescence intensities were calculated in GFP$^+$ and Thy1.1$^+$ cells. GFP$^+$ and Thy1.1$^+$ cells were also
497 counted in recovered cells (*H*). n=6 each group. ** $p$<0.01 (Mann-Whitney tests).

498 (*I*) Model: During $T_{reg}$ cell development, Tet enzymes demethylate the *Foxp3 cis*-regulatory elements,
499 specifically 12 CpG sites within enhancer CNS2, to stabilize Foxp3 transcription. This process is
500 accompanied by enhanced chromatin accessibility of CNS2 and association of CNS2 with Stat5 and
501 Foxp3. However, the contribution of Stat5 and Foxp3 binding at CNS2 to the stable, qualitative Foxp3
502 expression is minor, suggesting that the parallel circuits established by CNS2 demethylation act in a
503 partially redundant manner to maintain Foxp3 expression. Uncharacterized keystone factors in which
504 single deficiency may severely impair the stability of qualitative Foxp3 transcription could also govern
505 CNS2 function.

Figure 6

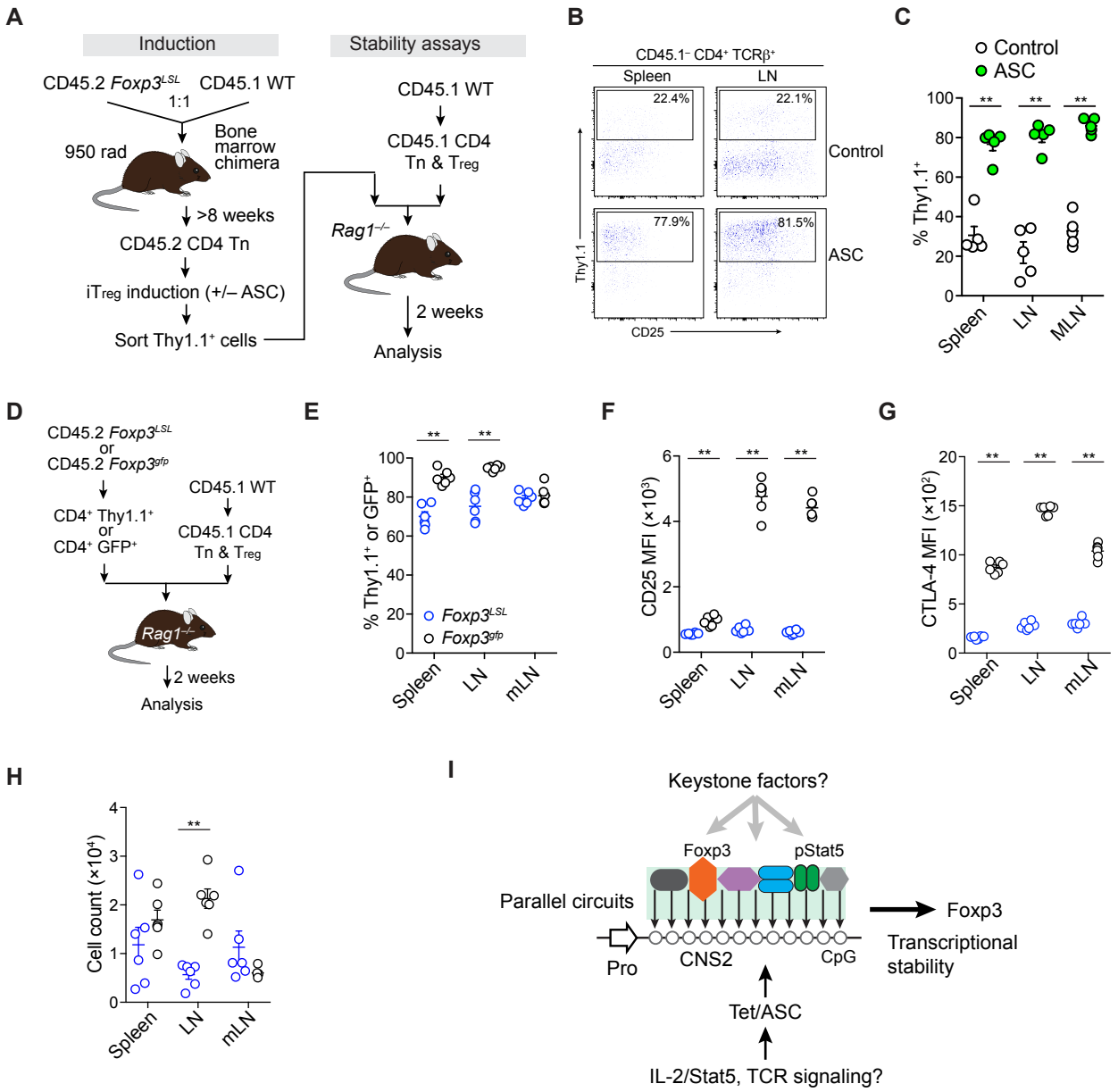
A
Induction
Stability assays
CD45.2 Foxp3LSL
CD45.1 WT
1:1
950 rad
Bone marrow chimera
>8 weeks
CD45.2 CD4 Tn
iTreg induction (+/– ASC)
Sort Thy1.1+ cells
CD45.1 WT
CD45.1 CD4 Tn & Treg
Rag1–/–
2 weeks
Analysis
B
CD45.1– CD4+ TCRβ+
Spleen
LN
22.4%
22.1%
77.9%
81.5%
Control
ASC
Thy1.1
CD25
C
Control
ASC
% Thy1.1+
Spleen
LN
MLN
D
CD45.2 Foxp3LSL
or
CD45.2 Foxp3gfp
CD4+ Thy1.1+
or
CD4+ GFP+
CD45.1 WT
CD45.1 CD4 Tn & Treg
Rag1–/–
2 weeks
Analysis
E
% Thy1.1+ or GFP+
Foxp3LSL
Foxp3gfp
Spleen
LN
mLN
F
CD25 MFI (×10³)
Spleen
LN
mLN
G
CTLA-4 MFI (×10²)
Spleen
LN
mLN
H
Cell count (×10⁴)
Spleen
LN
mLN
I
Keystone factors?
Foxp3
pStat5
Parallel circuits
Foxp3
Transcriptional stability
Pro
CNS2
CpG
Tet/ASC
IL-2/Stat5, TCR signaling?

506 **SUPPLEMENTARY INFORMATION**

507 **Fig. S1. Histone acetylation drives Foxp3 induction during $T_{reg}$ cell development *in vitro*.**

508 (*A*-*E*) Titrated amounts of I-CBP112 (*A*), SGC-CBP30 (*B*), I-BET151 (*C*), bromosporine (*D*), or PFI-1
509 (*E*) were added in culture media during $T_{reg}$ cell induction *in vitro*. Cells were harvested on day 4 to
510 analyze Foxp3 expression.

511 (*F*) Effect of JQ1, when added from day 3 to day 4 during $T_{reg}$ cell induction, on the median
512 fluorescence intensity of Foxp3, CD25, GITR, and CTLA-4 in $CD4^+Foxp3^+$ cells.

513 Data show means + SEMs of triplicates and represent 2 independent experiments. ***$p<0.001$
514 (unpaired, two-tailed *t* test).

515 Related to Fig. 1.

Figure S1

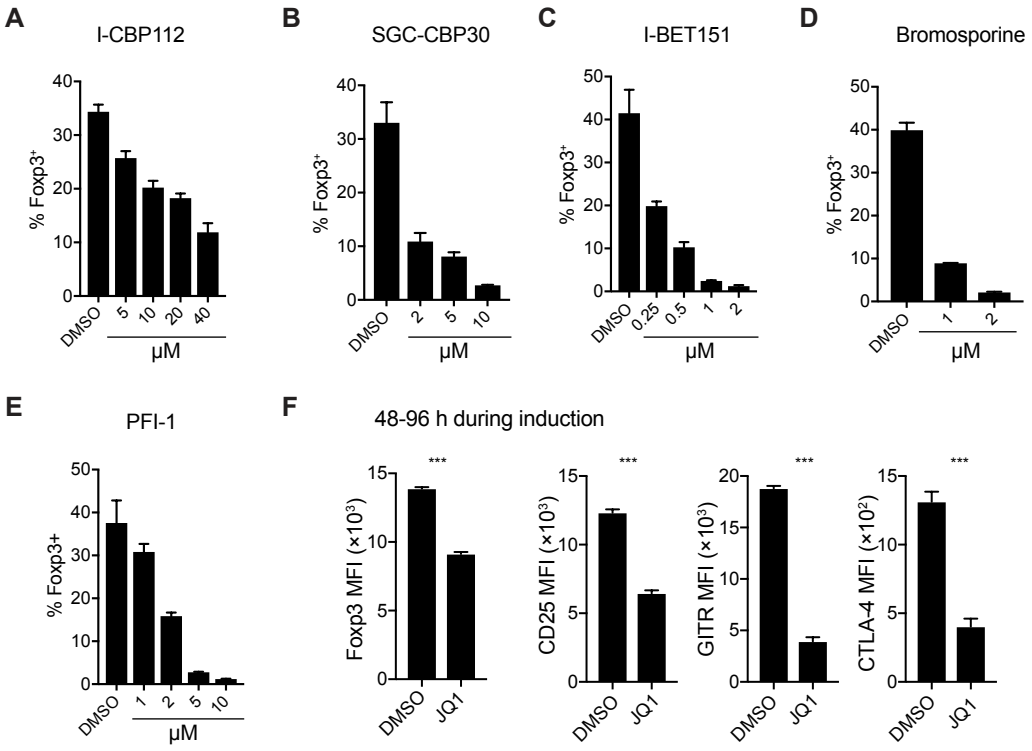
A
I-CBP112
% Foxp3+
DMSO
5
10
20
40
μM
B
SGC-CBP30
% Foxp3+
DMSO
2
5
10
μM
C
I-BET151
% Foxp3+
DMSO
0.25
0.5
1
2
μM
D
Bromosporine
% Foxp3+
DMSO
1
2
μM
E
PFI-1
% Foxp3+
DMSO
1
2
5
10
μM
F
48-96 h during induction
Foxp3 MFI (×10³)
CD25 MFI (×10³)
GITR MFI (×10³)
CTLA-4 MFI (×10²)
***
DMSO
JQ1

516 **Fig. S2. Effect of JQ1 on the stability of Foxp3 expression in $nT_{reg}$ and $iT_{reg}$ cells.**

517 (*A*) The $nT_{reg}$ cells doubled-sorted from *Foxp3*$^{gfp}$ mice were stimulated with beads coated with anti-CD3
518 and anti-CD28 antibodies in the presence of 500 U/mL recombinant IL-2 and either DMSO, IL-4, or
519 titrated amounts of JQ1 for 4 days. Live cells were gated to analyze Foxp3 expression. Data show
520 means + SEMs of triplicates and represent >2 independent experiments. ***$p$<0.001 (unpaired, two-
521 tailed *t* tests).

522 (*B*) Quantification of *Tet2* and *Tet3* deletion. CD4 Tn cells isolated from *Tet1-3*$^{fl/fl}$ mice were cultured in
523 $T_{reg}$-induction conditions. Cells were then transduced with vector or Cre-expressing retrovirus (reported
524 by Thy1.1 expression); 3-4 days later, Thy1.1$^{+}$ and Thy.1$^{-}$ cells were sorted for genomic DNA extraction
525 and qPCR. Data show means + SEMs of triplicates.

526 (*C*) Effect of *Tet*-deficiency and ASC treatment on Foxp3 induction efficiency. Data show means +
527 SEMs of triplicates and represent 2 independent experiments.

528 (*D*) Effect of *Tet*-deficiency and ASC treatment on CD25 expression in cells that maintained Foxp3
529 expression during $T_{reg}$ stability assay. Data show means + SEMs of triplicates and represent >2
530 independent experiments. ns, not significant, *$p$<0.05, ***$p$<0.001 (unpaired, two-tailed *t* test).

531 Related to Fig. 2.

Figure S2

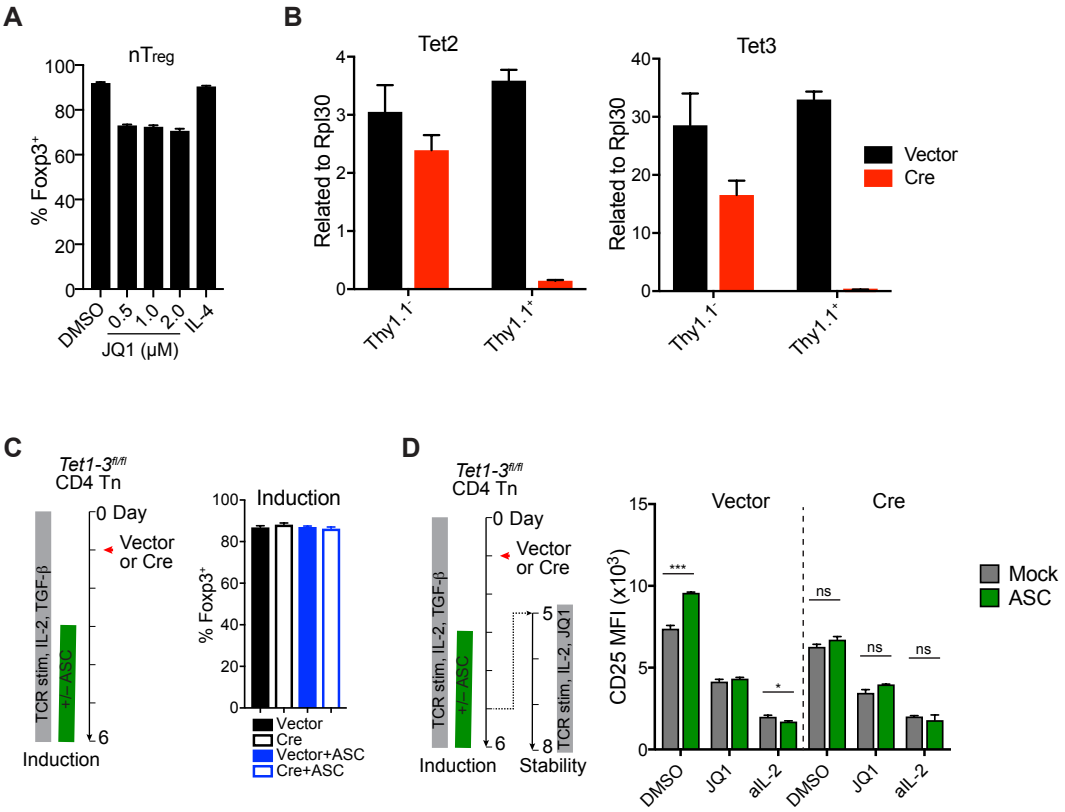
A
nTreg
% Foxp3+
100
80
60
40
20
0
DMSO
0.5
1.0
2.0
IL-4
JQ1 (μM)
B
Tet2
Related to Rpl30
Thy1.1-
Thy1.1+
Tet3
Vector
Cre
C
Tet1-3fl/fl
CD4 Tn
0 Day
Vector
or Cre
TCR stim, IL-2, TGF-β
+/- ASC
6
Induction
Induction
% Foxp3+
Vector
Cre
Vector+ASC
Cre+ASC
D
Tet1-3fl/fl
CD4 Tn
0 Day
Vector
or Cre
TCR stim, IL-2, TGF-β
+/- ASC
6
Induction
5
8
Stability
TCR stim, IL-2, JQ1
Vector
Cre
CD25 MFI (x10^3)
15
10
5
0
***
ns
*
ns
ns
DMSO
JQ1
aIL-2
DMSO
JQ1
aIL-2
Mock
ASC

532 **Fig. S3. Whole-genome bisulfite sequencing of $iT_{reg}$ cells treated with ASC.**

533 (*A*) Overall methylation fraction of CpG sites in CD4 Tn, $nT_{reg}$, Te, and mock- and ASC-treated $iT_{reg}$

534 cells. Whole-genome bisulfite sequencing was performed by using cells sorted from male *Foxp3*$^{gfp}$ mice

535 with or without being cultured *in vitro*. Data were merged from 2 biological replicates.

536 (*B*) Principal component analysis and clustering of the top 3000 most-variable CpG sites, explaining

537 73% of total variations (var).

538 Related to Fig. 3.

Figure S3

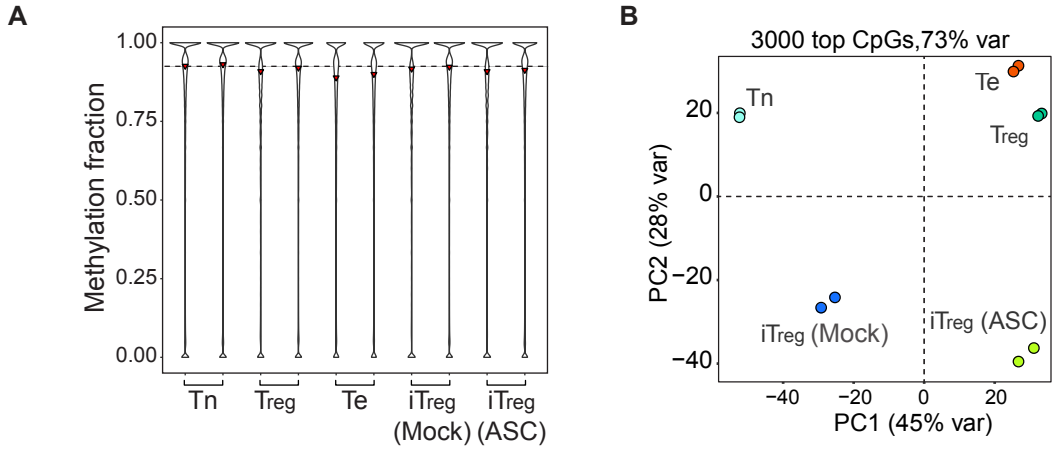
A
Methylation fraction
1.00
0.75
0.50
0.25
0.00
Tn
Treg
Te
iTreg (Mock)
iTreg (ASC)
B
3000 top CpGs,73% var
Tn
Te
Treg
iTreg (Mock)
iTreg (ASC)
PC2 (28% var)
PC1 (45% var)
20
0
−20
−40
−40
−20
0
20

539 **Fig. S4. Representative regions subjected to Tet/ASC–dependent DNA demethylation.**

540 (*A*) Differentially methylated CpG sites in ASC-treated $iT_{reg}$ and $nT_{reg}$ cells. Differences in mCpG levels
541 of $nT_{reg}$ and Te cells were plotted against those of mock- and ASC-treated $iT_{reg}$ cells. WGBS with 40×
542 coverage was performed by using cells derived from male *Foxp3*$^{gfp}$ mice. Data were merged from 2
543 biological replicates.

544 (*B*-*G*) Representative regions (highlighted) showing differences in mCpG levels of mock- and ASC-
545 treated $iT_{reg}$ cells. Vertical bars represent individual CpG sites; their heights indicate methylation levels
546 from 0 to 1. All samples were plotted at the same scale. Data were merged from 2 biological replicates.

547 Related to Fig. 4.

Figure S4

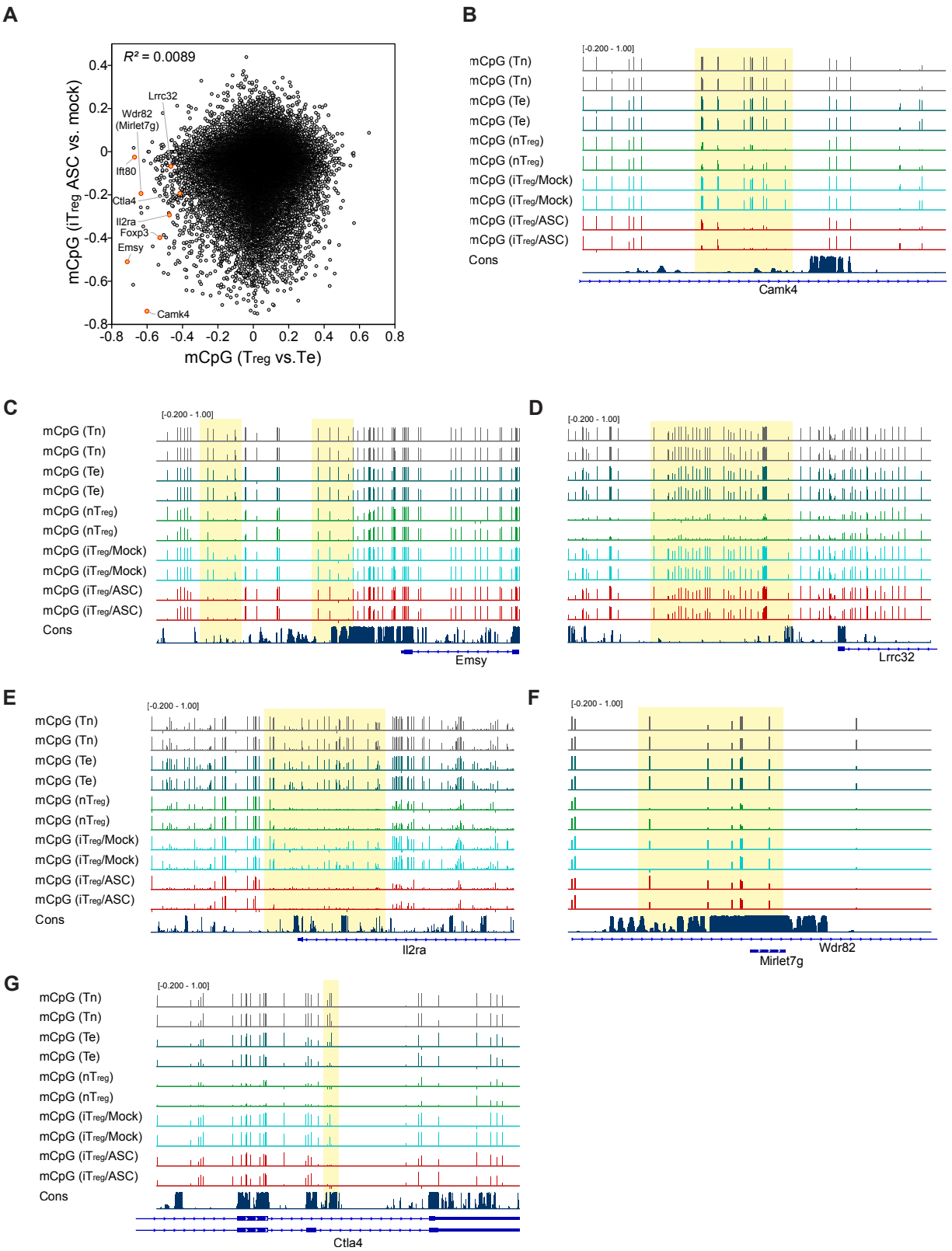
A
R² = 0.0089
Lrrc32
Wdr82
(Mirlet7g)
Ift80
Ctla4
Il2ra
Foxp3
Emsy
Camk4
mCpG (iTreg ASC vs. mock)
mCpG (Treg vs.Te)
B
[-0.200 - 1.00]
mCpG (Tn)
mCpG (Te)
mCpG (nTreg)
mCpG (iTreg/Mock)
mCpG (iTreg/ASC)
Cons
Camk4
C
Emsy
D
Lrrc32
E
Il2ra
F
Wdr82
Mirlet7g
G
Ctla4

548 **Fig. S5. Representative regions with differential CpG methylation and Stat5 binding.**

549 ATAC-seq, mCpG levels, and Stat5 ChIP-seq of $nT_{reg}$ and mock- and ASC-treated $iT_{reg}$ cells were
550 aligned with DNA sequence conservation. Regions undergoing differential DNA methylation and Stat5
551 binding are highlighted.

552 Related to Fig. 4.

Figure S5

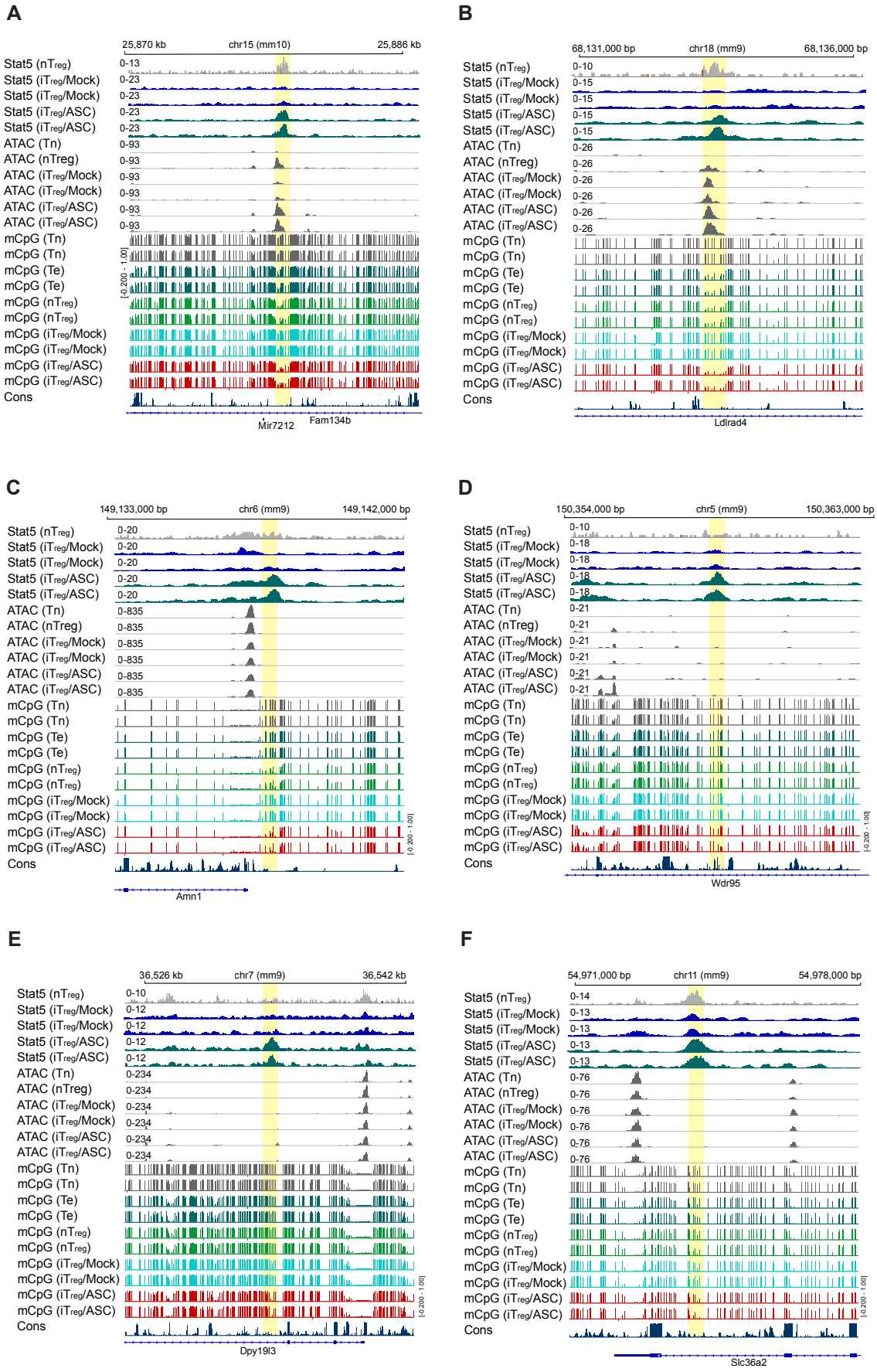
A
25,870 kb
chr15 (mm10)
25,886 kb
Stat5 (nTreg)
Stat5 (iTreg/Mock)
Stat5 (iTreg/Mock)
Stat5 (iTreg/ASC)
Stat5 (iTreg/ASC)
ATAC (Tn)
ATAC (nTreg)
ATAC (iTreg/Mock)
ATAC (iTreg/Mock)
ATAC (iTreg/ASC)
ATAC (iTreg/ASC)
mCpG (Tn)
mCpG (Tn)
mCpG (Te)
mCpG (Te)
mCpG (nTreg)
mCpG (nTreg)
mCpG (iTreg/Mock)
mCpG (iTreg/Mock)
mCpG (iTreg/ASC)
mCpG (iTreg/ASC)
Cons
[-0.200 - 1.00]
Mir7212
Fam134b
B
68,131,000 bp
chr18 (mm9)
68,136,000 bp
Ldlrad4
C
149,133,000 bp
chr6 (mm9)
149,142,000 bp
Amn1
D
150,354,000 bp
chr5 (mm9)
150,363,000 bp
Wdr95
E
36,526 kb
chr7 (mm9)
36,542 kb
Dpy19l3
F
54,971,000 bp
chr11 (mm9)
54,978,000 bp
Slc36a2

553 **Supplementary Table 1. Key resources used in this study.**

554 **MATERIALS AND METHODS**

555 **Mice**

556 All animal experiments were approved by St. Jude Children's Research Hospital's Institutional
557 Animal Care and Use Committee (approval number 612). All mice were maintained and bred in a
558 specific pathogen–free facility. Six- to twelve-week-old male and female mice were used for $T_{reg}$
559 experiments. Because the *Foxp3* gene is on the X-chromosome, which undergoes random inactivation
560 in females, male mice were used for epigenetic experiments, including whole-genome bisulfite
561 sequencing, chromatin accessibility, ChIP, and Cut&Run assays. *Foxp3*$^{gfp}$, *Foxp3*$^{\Delta CNS2\text{-}gfp}$, and *Tet1*$^{fl/fl}$
562 *Tet2*$^{fl/fl}$ *Tet3*$^{fl/fl}$ (*Tet1-3*$^{fl/fl}$) mice were described previously (Fontenot et al., 2005; Herzig et al., 2017;
563 Zheng et al., 2010). *Foxp3*$^{loxP\text{-}Thy1.1\text{-}Stop\text{-}loxP\text{-}gfp}$ (*Foxp3*$^{LSL}$) mice were generated by inserting the loxP-
564 Thy1.1-Stop-loxP-gfp cassette into a *Foxp3* intron before the coding sequence (Hu et al., submitted).

565 **T cell isolation and culture**

566 CD4 T cells from the lymph nodes and spleens were enriched via EasySep Mouse CD4 T Cell
567 Isolation Kits (STEMELL). CD4 naïve T cells (Tn, $CD4^+CD25^-CD44^-CD62L^{hi}$) and natural $T_{reg}$ cells
568 ($CD4^+GFP^+$) T cells were further sorted by FACS. T cells were cultured at 37°C, 5% $CO_2$ in complete
569 RPMI1640 medium (RPMI1640 supplemented with 10% fetal bovine serum [FBS], 2 mM L-glutamine, 1
570 mM sodium pyruvate, 1% non-essential amino acid, 10 mM HEPES, 20 μM 2-mercaptoethanol, 100
571 U/mL penicillin, and 100 mg/mL streptomycin) and indicated cytokines and compounds.

572 **$T_{reg}$ cell induction and stability assays**

573 Induction of $T_{reg}$ or wannabe $T_{reg}$ differentiation *in vitro* was conducted according to published
574 protocols (Feng et al., 2015; Yue et al., 2016). Briefly, plates or dishes were precoated with anti-CD3
575 and anti-CD28 antibodies (1 μg/mL) in PBS (Supplementary Table 1) at 37°C for 2 h to culture FACS-
576 sorted CD4 Tn cells from WT or *Foxp3*$^{LSL}$ mixed bone marrow chimeras in complete RPMI1640
577 supplemented with recombinant human IL-2 (100 U/mL) and recombinant human TGF-β (1 ng/mL) for

578 4 days with or without 0.25 mM ascorbic acid-2-phosphate or indicated compounds. To test the stability
579 of Foxp3 transcription, $iT_{reg}$ or wannabe $iT_{reg}$ cells that were sorted based on GFP-Foxp3 or Thy1.1
580 expression, respectively, after 4 days of induction were further cultured on plates pre-coated with anti-
581 CD3 and anti-CD28 antibodies (1 μg/mL each), recombinant human IL-2 (100 U/mL), IL-2 neutralization
582 antibodies (25 μg/mL each of JES6-54H and S4B6-1), or indicated cytokines or compounds for 4 more
583 days. The $nT_{reg}$ cells were cultured in the presence of Dynabeads Mouse T-Activator CD3/CD28
584 (Invitrogen) with 500 U/mL recombinant human IL-2 for 4 days and then given fresh media with
585 recombinant human IL-2 and indicated cytokines or compounds for 4 more days. CD4 Tn cells were
586 cultured on anti-CD3 and anti-CD28 antibody–coated plates or dishes with recombinant human IL-2 for
587 4 days to generate Th0 cells. After $T_{reg}$ induction or stability assays, cells were collected and stained
588 with viability dye and fluorophore-conjugated antibodies for flow-cytometry analysis.

589 **Flow-cytometry analysis**

590 Cell staining and flow-cytometry analyses were performed as we previously described (Feng et
591 al., 2014; Feng et al., 2015). Briefly, fluorophore-conjugated antibodies were used to stain cells
592 (Supplementary Table 1). Cells were first stained with fixable viability dye, then incubated with indicated
593 antibodies against cell surface markers followed by fixation/permeabilization with the
594 Foxp3/Transcription Factor Staining Buffer Set (eBioscience) and intracellular staining for Foxp3, if
595 needed. Cells were fixed in 1% paraformaldehyde for 10 min after staining. FACS analyses were
596 performed on LSRII or LSR Fortessa (BD Biosciences) flow cytometers; data were analyzed via FlowJo
597 (BD Biosciences).

598 **Retroviral packaging and transduction**

599 Retroviral packing and transduction of mouse primary T cells were conducted according to our
600 published protocols (Feng et al., 2015). Briefly, Platinum-E (Plat-E) cells were used to package the
601 retrovirus. Puromycin (1 μg/mL) and blasticidin (10 μg/mL) were added to the culture media to maintain

602 Plat-E cells according to the manufacturer's manual (Cell Biolabs); 24 h before transfection, cells were
603 seeded on new dishes in media without puromycin and blasticidin. Then, pMigR1-IRES-Thy1.1 or
604 pMigR1-Cre-IRES-Thy1.1 plasmid (Feng et al., 2015) and pCI-Eco were cotransfected into these cells
605 with TransIT-293 Transfection Reagent (Mirus); 2-3 days after transfection, viral supernatant was
606 collected and filtered with 0.45-μm syringe filters, aliquoted, and stored at -80°C.

607 **Bisulfite sequencing**

608 Cells used for bisulfite sequencing were sorted from male *Foxp3*$^{gfp}$ mice with or without *in vitro*
609 culture. The following markers were used to sort cells: for Tn, CD4$^{+}$GFP$^{-}$CD25$^{-}$CD44$^{lo}$CD62L$^{hi}$; for Te,
610 CD4$^{+}$GFP$^{-}$CD44$^{hi}$CD62L$^{lo}$; and for $T_{reg}$, CD4$^{+}$GFP$^{+}$. Genomic DNA was prepared from sorted cells by
611 proteinase K digestion followed by phenol:chloroform:isoamyl alcohol extraction and 2-propanol
612 precipitation. More than 100 ng of genomic DNA in each sample was converted via EpiTect Bisulfite
613 Kits (Qiagen). Bisulfite conversion efficiency was tested via PCR and Sanger sequencing of *Foxp3*
614 enhancer CNS2 as we previously described(Feng et al., 2014). To perform whole-genome bisulfite
615 sequencing, libraries were prepared from converted DNA by using the Accel-NGS Methyl-Seq DNA
616 Library Kit (Swift Biosciences), analyzed for insert size distribution on a 2100 BioAnalyzer (Agilent
617 Technologies,), and quantified by using the Quant-iT PicoGreen ds DNA assay (Life Technologies).
618 Paired-end, 100-cycle sequencing was performed on a Hi-seq 4000 (Illumina) to achieve an average
619 40× coverage.

620 Bisulfite sequencing data were aligned to mouse genome mm9 by using BSMAP2.74 (Xi & Li,
621 2009). The methylation ratio for each CpG site was extracted by methratio.py from BSMAP2.74. The
622 methylation ratio was then converted to bw file for visualization. The M values for the 3,000 most
623 variable CpG sites were used for hierarchical clustering and PCA analyses. M value = $\log_2$(C count/T
624 count) at a CpG site (an offset value of 0.5 was added).

625 **ATAC Sequencing**

626 ATAC-Seq was performed as previously reported (Buenrostro, Wu, Chang, & Greenleaf, 2015).
627 Briefly, $5\times10^4$ cells were FACS sorted and lysed in 300 μL of ice-cold lysis buffer (10 mM Tris-HCl, pH
628 7.5, 10 mM NaCl, 3 mM $MgCl_2$, 0.1% NP-40). After centrifugation, the supernatant was removed; 50 μL
629 of reaction mix containing 25 μL of TD buffer, 2.5 μL of TDE1 (Illumina Nextera DNA Library
630 Preparation Kit), and 22.5 μL of nuclease-free water was immediately added to perform transposition at
631 42°C for 40 min. DNA was purified by using the NucleoSpin Gel and PCR Clean-up kit (MACHEREY-
632 NAGEL). The transposed DNA was amplified by PCR for 10-12 cycles by using the Nextera DNA
633 Library Preparation Kit and Nextera XT Indexing Kit (Illumina). The library DNA within the 150- to 500-
634 bp range was enriched by AMPure XP beads (Beckman Coulter), quantified by NEBNext Library Quant
635 Kit (NEB), and sequenced with paired-end 100-cycles on a HiSeq 4000 sequencer (Illumina).

636 Paired-end reads of 100bp were trimmed by cutadapt (version 1.9, paired-end mode, default
637 parameter with "-m 25 -O 6") (Martin, 2011) and aligned to mouse genome mm9 (MGSCv37 from
638 Sanger) by BWA (version 0.7.12-r1039, default parameter)(H. Li & Durbin, 2009). Duplicate reads were
639 marked by biobambam2 (version v2.0.87)(Tischler & Leonard, 2014); non-duplicate, properly paired
640 reads were kept by samtools (parameter "-q 1 -F 1804" version 1.2)(H. Li et al., 2009). To adjust Tn5
641 shift, reads were offset by +4 bp for the sense strand and -5 bp for the antisense strand. We used
642 fragment size to separate reads into nucleosome-free, mononucleosome, dinucleosome, and
643 trinucleosome groups as described (Buenrostro et al., 2013) and generated bw files by using the center
644 80 bp of fragments and scale to 20 million nucleosome-free reads. Two replicates were merged to
645 enhance peak calling by MACS2 (version 2.1.1.20160309 default parameters with "--extsize 200 --
646 nomodel ")(Zhang et al., 2008). All of the important nucleosome-free regions were considered to have
647 been called if a sample had more than 15 million nucleosome-free reads after merging. To ensure
648 reproducibility, we first merged peaks from different cell types to create a set of reference chromatin-
649 accessible regions. We then used bedtools (v2.24.0)(Quinlan & Hall, 2010) to count nucleosome-free
650 reads from each sample to overlay with the reference regions. To identify differentially accessible

651 regions, we first normalized raw nucleosome-free reads counts by using trimmed mean of M-values
652 (TMM) and then applied empirical Bayes statistics testing after linear fitting with voom package (R 3.23,
653 edgeR 3.12.1, limma 3.26.9)(Law, Chen, Shi, & Smyth, 2014). A false discovery rate (FDR)–adjusted *p*-
654 value <0.05 and fold change > 2 were used as cutoff values for differentially accessible regions.

655 **ChIP qPCR and sequencing**

656 CD4 Tn cells from *Foxp3*$^{gfp}$ male mice were induced to become $iT_{reg}$ or Th0 cells in the presence
657 or absence of 0.25 mM ascorbic acid-2-phosphate. The $nT_{reg}$ cells from *Foxp3*$^{gfp}$ male mice were FACS
658 sorted and expanded *in vitro* for 5 days by using Dynabeads Mouse T-Activator CD3/CD28 (Invitrogen)
659 in the presence of 500 U/mL recombinant IL-2. To perform Stat5 ChIP, $iT_{reg}$ or $nT_{reg}$ cells were starved
660 for 3 h in complete RPMI1640 without cytokines. Cells were then restimulated with 500 U/mL IL-2 for 30
661 min. A two-step protocol was used to fix the cells as we previously described (Feng et al., 2014). In
662 brief, cells were resuspended at $5\times10^6$ cells/mL in 1 mM $MgCl_2$/PBS and treated with 2 mM DSG cross-
663 linker (Thermo Fisher Scientific) at room temperature for 30 min on a rotator. Cells were then washed
664 twice with PBS and fixed with 1% formaldehyde at room temperature for 5 min. Fixation was quenched
665 by adding 125 mM glycine. Cells were washed once with ice-cold PBS, aliquoted, and either frozen at -
666 80°C or immediately processed by downstream reactions. Chromatin sonication was performed by
667 using the truChIP Chromatin Shearing Kit (Covaris) with Focused-Ultrasonicator M220 (Corvaris)
668 following the manufacturer's instructions. Chromatin was sheared to 400-800 bp for Stat5 and Foxp3
669 ChIP; 10% of samples were aliquoted as input control. In each ChIP reaction, 5 µL of rabbit anti-Stat5
670 (CST), 10 µL of rabbit anti-Foxp3 (Abcam), or control rabbit IgG (CST) were added to the lysis/binding
671 buffer (50 mM HEPES pH 8.0, 1 mM EDTA, 1% Triton X-100, 0.1% sodium deoxycholate, 0.1% SDS,
672 140 mM NaCl, 1 mM PMSF, and protease inhibitor cocktail) to precipitate the chromatin. After an
673 overnight incubation, protein A and protein G magnetic beads (Invitrogen) were added to capture the
674 antibody-chromatin complexes. Next, beads were washed according to our published protocols (Feng
675 et al., 2014). To release the DNA, ChIP samples were treated with proteinase K, followed by

676 phenol:chloroform:isoamyl alcohol extraction and 2-propanol precipitation in the presence of GlycoBlue
677 Coprecipitant (Invitrogen). DNA pellets were dissolved in 1×TE buffer (10 mM Tris HCl pH 8.0, 1 mM
678 EDTA) for qPCR or deep sequencing.

679 To quantify the precipitated DNA, qPCR was performed with locus- or region-specific primers,
680 PowerUp SYBR Green Master Mix (Applied Biosystems), and the CFX384 Real Time PCR System
681 (Bio-Rad). Relative enrichment of the targets was calculated by normalizing the signals of the
682 precipitated DNA to those of the input samples. To perform ChIP-Seq, libraries were prepared with
683 precipitated DNA by using the KAPA Hyper Prep Kit (Kapa Biosystems). The library DNA was enriched
684 by size selection with AMPure XP beads and quantified by using the NEBNext Library Quant Kit.
685 Indexed samples were pooled together for 100 cycles of paired end sequencing on a HiSeq 4000 or
686 HiSeq 2500 system (Illumina). More than 40 million reads per sample were sequenced for downstream
687 analysis.

688 Single-end reads of 50 bp were mapped to mouse genome mm9 (MGSCv37 from Sanger) by
689 BWA (version 0.7.12-r1039, default parameter)(H. Li & Durbin, 2009). Duplicate reads were marked
690 with biobambam2 (version v2.0.87)(Tischler & Leonard, 2014); non-duplicate reads were kept by
691 samtools (parameter "-q 1 -F 1024" version 1.2) (H. Li et al., 2009). We followed ENCODE guidelines to
692 assess the quality of our data as previously described(Yang et al., 2019). Next, we extended reads to
693 fragment size (detected by SPP v1.1)(Kharchenko, Tolstorukov, & Park, 2008) and generated bw
694 tracks (normalized to 10 million uniquely mapped reads) for visualization. We used MACS2 (version
695 2.1.1.20160309, parameters "--nomodel --extsize fragment size") to call peaks. To assure
696 reproducibility, we finalized the peaks for each group if they were called with a stringent cutoff value
697 (FDR-adjusted $p$-value < 0.05 in MACS2) in one sample and at least called with a lower cutoff value
698 (FDR-corrected $p$-value < 0.5 in MACS2) in the other. Peaks were further merged between groups.
699 Reads were extended to fragment size for each sample via bedtools (v2.24.0)(Quinlan & Hall, 2010).
700 We used correlation plots to assess reproducibility among replicates. After TMM normalization, we

701 used empirical Bayes statistics testing after linear fitting from voom package(R 3.23, edgeR 3.12.1,
702 limma 3.26.9)(Law et al., 2014) to identify differential binding sites. FDR-adjusted *p*-value <0.05 and
703 fold change > 2 were used as cutoff values.

704 **Quantification of nascent RNA**

705 Cells were labeled with 0.5 mM ethylene uridine for 45 min ($2.5 \times 10^6$ cells/mL culture medium)
706 before being lysed with TRIzol according to the manufacturer's protocol (Thermo Fisher Scientific).
707 Total RNA was isolated via chloroform separation and 2-propanol precipitation; 1 µg RNA was then
708 used to perform the click reaction followed by a purification with Dynabeads MyOne Streptavidin T1
709 beads according to the manufacturer's protocol (Click-iT Nascent RNA Capture Kit, Thermo Fisher
710 Scientific). Enriched nascent RNA was immediately used as a template to generate cDNA with the
711 SuperScript VILO cDNA Synthesis Kit (Thermo Fisher Scientific). Quantification of Foxp3 transcripts
712 was conducted with specific primers on the CFX384 Real Time PCR System (Bio-Rad).

713 **Mixed bone marrow chimeras**

714 Mixed bone marrow chimeric mice were generated as we previously described (Feng et al.,
715 2015). Briefly, recipient mice ($CD45.1^+CD45.2^+$) were lethally irradiated (9.5 Gy) 24 h before
716 intravenous injection of $5 \times 10^6$ to $10 \times 10^6$ bone marrow cells from CD45.1 WT and CD45.2 *Foxp3*$^{LSL}$
717 mixed at a 1:1 ratio. After bone marrow transfer, the recipient mice were administered neomycin (2
718 mg/mL) in drinking water for 3 weeks and euthanized for CD4 T cell preparations 8-10 weeks later.

719 **Cut&Run experiments**

720 Viable $iT_{reg}$ cells were sorted by *Foxp3*$^{gfp}$ reporter expression after induction. Cut&Run was
721 performed as described (Skene & Henikoff, 2017). Briefly, $1\times10^6$ $iT_{reg}$ cells were first attached to
722 Concanavalin A (ConA)-coated magnetic beads, permeabilized with digitonin-wash buffer (20 mM
723 HEPES, pH7.5, 150 mM NaCl, 0.5 mM spermidine, 0.01% Digitonin, and protease inhibitors), and then
724 incubated with antibody (1:100 H3K27ac) for 2 h at 4°C on a rotator. The beads-cell mixture was

725 washed thrice with digitonin-wash buffer, resuspended in 200 μL of protein A-MNase, and incubated for
726 1 h at 4°C on a rotator. After 3 rounds of washing, beads were resuspended in 150 μL of digitonin-wash
727 buffer and chilled in an ice-water bath for 5 min; 3 μL of 100 mM $CaCl_2$ was added into the tubes with
728 gentle vortexing, and the beads were incubated in an ice-water bath for 30 min. Next, 150 μL of
729 2×STOP buffer (170 mM NaCl, 20 mM EDTA, 20 mM EGTA, 0.05% Digitonin, 20 mg/mL GlycoBlue, 25
730 mg/mL RNase A) was added and incubated at 37°C for 30 min. After clarification on a magnet stand,
731 supernatant was transferred to a fresh tube for phenol:chloroform extraction and ethanol precipitation.
732 A library was prepared by using KAPA Hyper Prep Kit, and 5ng DNA was loaded for deep sequencing.

733 After adapter trimming by cutadapt (version 1.9, paired-end mode, default parameter with " -m
734 25 -O 6 ")(Martin, 2011), 50-bp paired-end reads were mapped to mouse genome mm9 (MGSCv37
735 from Sanger) by using BWA (version 0.7.12-r1039, default parameter)(H. Li & Durbin, 2009). Duplicate
736 reads were marked with biobambam2 (version v2.0.87)(Tischler & Leonard, 2014); non-duplicate reads
737 were kept by samtools (parameter "-q 1 -F 1804" version 1.2)(H. Li et al., 2009). At least 5 million reads
738 per sample were used for further analysis, as suggested in published research (Skene, Henikoff, &
739 Henikoff, 2018). We generated bw files using the center 80 bp of fragments smaller than 2000 bp and
740 normalizing the reads counts to 10 million fragments.

741 **RNA sequencing**

742 $T_{reg}$ cells induced from male WT *Foxp3*$^{gfp}$ CD4 Tn cells in the presence or absence of 0.25 mM
743 ascorbic acid-2-phosphate were sorted on day 4 during culture. Cells were lysed with TRIzol; RNA was
744 extracted, and sequencing libraries were constructed by using SMARTer cDNA synthesis kits (Takara).
745 Libraries were sequenced by using the HiSeq 2500 platform (Illumina) according to a standard paired-
746 end protocol. Reads processing, mapping, and differential gene expression analyses were performed
747 as we previously described[25].

748 **Data resources**

749 The sequencing data have been deposited at https://www.ncbi.nlm.nih.gov/geo/ with access
750 number GSE146250.

751 **Software resources**

752 The R codes used for the analyses are available upon request.

753 **REFERENCES**


754 Brunkow, M. E., Jeffery, E. W., Hjerrild, K. A., Paeper, B., Clark, L. B., Yasayko, S. A., . . . Ramsdell, F.
755 (2001). Disruption of a new forkhead/winged-helix protein, scurfin, results in the fatal
756 lymphoproliferative disorder of the scurfy mouse. *Nat Genet, 27*(1), 68-73. doi:10.1038/83784
757 Buenrostro, J. D., Giresi, P. G., Zaba, L. C., Chang, H. Y., & Greenleaf, W. J. (2013). Transposition of
758 native chromatin for fast and sensitive epigenomic profiling of open chromatin, DNA-binding
759 proteins and nucleosome position. *Nat Methods, 10*(12), 1213-1218. doi:10.1038/nmeth.2688
760 Buenrostro, J. D., Wu, B., Chang, H. Y., & Greenleaf, W. J. (2015). Atac-seq: A method for assaying
761 chromatin accessibility genome-wide. *Curr Protoc Mol Biol, 109*, 21 29 21-29.
762 doi:10.1002/0471142727.mb2129s109
763 Chinen, T., Kannan, A. K., Levine, A. G., Fan, X., Klein, U., Zheng, Y., . . . Rudensky, A. Y. (2016). An
764 essential role for the il-2 receptor in treg cell function. *Nat Immunol, 17*(11), 1322-1333.
765 doi:10.1038/ni.3540
766 Fan, M. Y., Low, J. S., Tanimine, N., Finn, K. K., Priyadharshini, B., Germana, S. K., . . . Turka, L. A.
767 (2018). Differential roles of il-2 signaling in developing versus mature tregs. *Cell Rep, 25*(5),
768 1204-1213 e1204. doi:10.1016/j.celrep.2018.10.002
769 Feng, Y., Arvey, A., Chinen, T., van der Veeken, J., Gasteiger, G., & Rudensky, A. Y. (2014). Control of
770 the inheritance of regulatory t cell identity by a cis element in the foxp3 locus. *Cell, 158*(4), 749-
771 763. doi:10.1016/j.cell.2014.07.031
772 Feng, Y., van der Veeken, J., Shugay, M., Putintseva, E. V., Osmanbeyoglu, H. U., Dikiy, S., . . .
773 Rudensky, A. Y. (2015). A mechanism for expansion of regulatory t-cell repertoire and its role in
774 self-tolerance. *Nature, 528*(7580), 132-136. doi:10.1038/nature16141
775 Fontenot, J. D., Gavin, M. A., & Rudensky, A. Y. (2003). Foxp3 programs the development and function
776 of cd4+cd25+ regulatory t cells. *Nat Immunol, 4*(4), 330-336. doi:10.1038/ni904

Fontenot, J. D., Rasmussen, J. P., Williams, L. M., Dooley, J. L., Farr, A. G., & Rudensky, A. Y. (2005). Regulatory t cell lineage specification by the forkhead transcription factor foxp3. *Immunity, 22*(3), 329-341. doi:10.1016/j.immuni.2005.01.016

Fu, W., Ergun, A., Lu, T., Hill, J. A., Haxhinasto, S., Fassett, M. S., . . . Benoist, C. (2012). A multiply redundant genetic switch 'locks in' the transcriptional signature of regulatory t cells. *Nat Immunol, 13*(10), 972-980. doi:10.1038/ni.2420

Fujisawa, T., & Filippakopoulos, P. (2017). Functions of bromodomain-containing proteins and their roles in homeostasis and cancer. *Nat Rev Mol Cell Biol, 18*(4), 246-262. doi:10.1038/nrm.2016.143

Gavin, M., & Rudensky, A. (2003). Control of immune homeostasis by naturally arising regulatory cd4+ t cells. *Curr Opin Immunol, 15*(6), 690-696. doi:S0952791503001481 [pii]

Gavin, M. A., Rasmussen, J. P., Fontenot, J. D., Vasta, V., Manganiello, V. C., Beavo, J. A., & Rudensky, A. Y. (2007). Foxp3-dependent programme of regulatory t-cell differentiation. *Nature, 445*(7129), 771-775. doi:10.1038/nature05543

Ghosh, S., Roy-Chowdhuri, S., Kang, K., Im, S. H., & Rudra, D. (2018). The transcription factor foxp1 preserves integrity of an active foxp3 locus in extrathymic treg cells. *Nat Commun, 9*(1), 4473. doi:10.1038/s41467-018-07018-y

Herzig, Y., Nevo, S., Bornstein, C., Brezis, M. R., Ben-Hur, S., Shkedy, A., . . . Abramson, J. (2017). Transcriptional programs that control expression of the autoimmune regulator gene aire. *Nat Immunol, 18*(2), 161-172. doi:10.1038/ni.3638

Hori, S., Nomura, T., & Sakaguchi, S. (2003). Control of regulatory t cell development by the transcription factor foxp3. *Science, 299*(5609), 1057-1061. doi:10.1126/science.1079490

Josefowicz, S. Z., Lu, L. F., & Rudensky, A. Y. (2012). Regulatory t cells: Mechanisms of differentiation and function. *Annu Rev Immunol, 30*, 531-564. doi:10.1146/annurev.immunol.25.022106.141623

802 Kharchenko, P. V., Tolstorukov, M. Y., & Park, P. J. (2008). Design and analysis of chip-seq
803 experiments for DNA-binding proteins. *Nat Biotechnol, 26*(12), 1351-1359. doi:10.1038/nbt.1508
804 Kim, H. P., & Leonard, W. J. (2007). Creb/atf-dependent t cell receptor-induced foxp3 gene expression:
805 A role for DNA methylation. *J Exp Med, 204*(7), 1543-1551. doi:10.1084/jem.20070109
806 Kim, J. M., Rasmussen, J. P., & Rudensky, A. Y. (2007). Regulatory t cells prevent catastrophic
807 autoimmunity throughout the lifespan of mice. *Nat Immunol, 8*(2), 191-197. doi:10.1038/ni1428
808 Law, C. W., Chen, Y., Shi, W., & Smyth, G. K. (2014). Voom: Precision weights unlock linear model
809 analysis tools for rna-seq read counts. *Genome Biol, 15*(2), R29. doi:10.1186/gb-2014-15-2-r29
810 Li, H., & Durbin, R. (2009). Fast and accurate short read alignment with burrows-wheeler transform.
811 *Bioinformatics, 25*(14), 1754-1760. doi:10.1093/bioinformatics/btp324
812 Li, H., Handsaker, B., Wysoker, A., Fennell, T., Ruan, J., Homer, N., . . . Genome Project Data
813 Processing, S. (2009). The sequence alignment/map format and samtools. *Bioinformatics,*
814 *25*(16), 2078-2079. doi:10.1093/bioinformatics/btp352
815 Li, X., Liang, Y., LeBlanc, M., Benner, C., & Zheng, Y. (2014). Function of a foxp3 cis-element in
816 protecting regulatory t cell identity. *Cell, 158*(4), 734-748. doi:10.1016/j.cell.2014.07.030
817 Liston, A., Farr, A. G., Chen, Z., Benoist, C., Mathis, D., Manley, N. R., & Rudensky, A. Y. (2007). Lack
818 of foxp3 function and expression in the thymic epithelium. *J Exp Med, 204*(3), 475-480.
819 doi:jem.20062465 [pii]

820 10.1084/jem.20062465
821 Liu, Y., Wang, L., Han, R., Beier, U. H., Akimova, T., Bhatti, T., . . . Hancock, W. W. (2014). Two
822 histone/protein acetyltransferases, cbp and p300, are indispensable for foxp3+ t-regulatory cell
823 development and function. *Mol Cell Biol, 34*(21), 3993-4007. doi:10.1128/MCB.00919-14
824 Malek, T. R., & Castro, I. (2010). Interleukin-2 receptor signaling: At the interface between tolerance
825 and immunity. *Immunity, 33*(2), 153-165. doi:10.1016/j.immuni.2010.08.004

826 Martin, M. (2011). Cutadapt removes adapter sequences from high-throughput sequencing reads.
827 *EMBnet.journal, 17*, -10-12.
828 Maruyama, T., Konkel, J. E., Zamarron, B. F., & Chen, W. (2011). The molecular mechanisms of foxp3
829 gene regulation. *Semin Immunol, 23*(6), 418-423. doi:10.1016/j.smim.2011.06.005
830 Nakatsukasa, H., Oda, M., Yin, J., Chikuma, S., Ito, M., Koga-Iizuka, M., . . . Yoshimura, A. (2019).
831 Loss of tet proteins in regulatory t cells promotes abnormal proliferation, foxp3 destabilization
832 and il-17 expression. *Int Immunol, 31*(5), 335-347. doi:10.1093/intimm/dxz008
833 Ohkura, N., Hamaguchi, M., Morikawa, H., Sugimura, K., Tanaka, A., Ito, Y., . . . Sakaguchi, S. (2012).
834 T cell receptor stimulation-induced epigenetic changes and foxp3 expression are independent
835 and complementary events required for treg cell development. *Immunity, 37*(5), 785-799.
836 doi:10.1016/j.immuni.2012.09.010
837 Ouyang, W., Beckett, O., Ma, Q., Paik, J. H., DePinho, R. A., & Li, M. O. (2010). Foxo proteins
838 cooperatively control the differentiation of foxp3+ regulatory t cells. *Nat Immunol, 11*(7), 618-
839 627. doi:ni.1884 [pii]

840 10.1038/ni.1884

841 Polansky, J. K., Kretschmer, K., Freyer, J., Floess, S., Garbe, A., Baron, U., . . . Huehn, J. (2008). DNA
842 methylation controls foxp3 gene expression. *Eur J Immunol, 38*(6), 1654-1663.
843 doi:10.1002/eji.200838105
844 Polansky, J. K., Schreiber, L., Thelemann, C., Ludwig, L., Kruger, M., Baumgrass, R., . . . Huehn, J.
845 (2010). Methylation matters: Binding of ets-1 to the demethylated foxp3 gene contributes to the
846 stabilization of foxp3 expression in regulatory t cells. *J Mol Med (Berl), 88*(10), 1029-1040.
847 doi:10.1007/s00109-010-0642-1
848 Quinlan, A. R., & Hall, I. M. (2010). Bedtools: A flexible suite of utilities for comparing genomic features.
849 *Bioinformatics, 26*(6), 841-842. doi:10.1093/bioinformatics/btq033

850 Rubtsov, Y. P., Niec, R. E., Josefowicz, S., Li, L., Darce, J., Mathis, D., . . . Rudensky, A. Y. (2010).
851 Stability of the regulatory t cell lineage in vivo. *Science, 329*(5999), 1667-1671.
852 doi:10.1126/science.1191996
853 Rudensky, A. Y. (2011). Regulatory t cells and foxp3. *Immunol Rev, 241*(1), 260-268.
854 doi:10.1111/j.1600-065X.2011.01018.x
855 Rudra, D., Egawa, T., Chong, M. M., Treuting, P., Littman, D. R., & Rudensky, A. Y. (2009). Runx-
856 cbfbeta complexes control expression of the transcription factor foxp3 in regulatory t cells. *Nat*
857 *Immunol, 10*(11), 1170-1177. doi:10.1038/ni.1795
858 Sakaguchi, S., Mikami, N., Wing, J. B., Tanaka, A., Ichiyama, K., & Ohkura, N. (2020). Regulatory t
859 cells and human disease. *Annu Rev Immunol*. doi:10.1146/annurev-immunol-042718-041717
860 Samstein, R. M., Arvey, A., Josefowicz, S. Z., Peng, X., Reynolds, A., Sandstrom, R., . . . Rudensky, A.
861 Y. (2012). Foxp3 exploits a pre-existent enhancer landscape for regulatory t cell lineage
862 specification. *Cell, 151*(1), 153-166. doi:10.1016/j.cell.2012.06.053
863 Sasidharan Nair, V., Song, M. H., & Oh, K. I. (2016). Vitamin c facilitates demethylation of the foxp3
864 enhancer in a tet-dependent manner. *J Immunol, 196*(5), 2119-2131.
865 doi:10.4049/jimmunol.1502352
866 Savage, P. A., Klawon, D. E. J., & Miller, C. H. (2020). Regulatory t cell development. *Annu Rev*
867 *Immunol*. doi:10.1146/annurev-immunol-100219-020937
868 Shrestha, S., Yang, K., Guy, C., Vogel, P., Neale, G., & Chi, H. (2015). Treg cells require the
869 phosphatase pten to restrain th1 and tfh cell responses. *Nat Immunol, 16*(2), 178-187.
870 doi:10.1038/ni.3076
871 Skene, P. J., Henikoff, J. G., & Henikoff, S. (2018). Targeted in situ genome-wide profiling with high
872 efficiency for low cell numbers. *Nat Protoc, 13*(5), 1006-1019. doi:10.1038/nprot.2018.015
873 Skene, P. J., & Henikoff, S. (2017). An efficient targeted nuclease strategy for high-resolution mapping
874 of DNA binding sites. *Elife, 6*. doi:10.7554/eLife.21856

875 Tischler, G., & Leonard, S. (2014). Biobambam: Tools for read pair collation based algorithms on bam
876 files. *Source Code for Biology and Medicine, 9*, 13-13. doi:10.1186/1751-0473-9-13
877 Urban, E. A., & Johnston, R. J., Jr. (2018). Buffering and amplifying transcriptional noise during cell fate
878 specification. *Front Genet, 9*, 591. doi:10.3389/fgene.2018.00591
879 Xi, Y., & Li, W. (2009). Bsmap: Whole genome bisulfite sequence mapping program. *BMC*
880 *Bioinformatics, 10*, 232. doi:10.1186/1471-2105-10-232
881 Yang, X., Xu, B., Mulvey, B., Evans, M., Jordan, S., Wang, Y. D., . . . Peng, J. C. (2019). Differentiation
882 of human pluripotent stem cells into neurons or cortical organoids requires transcriptional co-
883 regulation by utx and 53bp1. *Nat Neurosci, 22*(3), 362-373. doi:10.1038/s41593-018-0328-5
884 Yue, X., Lio, C. J., Samaniego-Castruita, D., Li, X., & Rao, A. (2019). Loss of tet2 and tet3 in regulatory
885 t cells unleashes effector function. *Nat Commun, 10*(1), 2011. doi:10.1038/s41467-019-09541-y
886 Yue, X., Trifari, S., Aijo, T., Tsagaratou, A., Pastor, W. A., Zepeda-Martinez, J. A., . . . Rao, A. (2016).
887 Control of foxp3 stability through modulation of tet activity. *J Exp Med, 213*(3), 377-397.
888 doi:10.1084/jem.20151438
889 Zhang, Y., Liu, T., Meyer, C. A., Eeckhoute, J., Johnson, D. S., Bernstein, B. E., . . . Liu, X. S. (2008).
890 Model-based analysis of chip-seq (macs). *Genome Biol, 9*(9), R137. doi:10.1186/gb-2008-9-9-
891 r137
892 Zheng, Y., Josefowicz, S., Chaudhry, A., Peng, X. P., Forbush, K., & Rudensky, A. Y. (2010). Role of
893 conserved non-coding DNA elements in the foxp3 gene in regulatory t-cell fate. *Nature,*
894 *463*(7282), 808-812. doi:10.1038/nature08750

895

## Supplementary Table 1

| REAGENT or RESOURCE | SOURCE | IDENTIFIER |
|---|---|---|
| **Antibodies** | | |
| AF488 anti-CD90.1(Thy1.1) (Clone: OX-7) | BioLegend | Cat#202506 |
| APC anti-CD44 (Clone: IM7) | eBioscience | Cat#17-0441-82 |
| Biotin anti-CD90.1(Thy1.1) (Clone: OX-7) | BioLegend | Cat#202510 |
| BV711 anti-CD4 (Clone: RM4-5) | BioLegend | Cat#100550 |
| BV785 anti-CD25 (Clone: PC61) | BioLegend | Cat#102017 |
| CD45.1 (Clone: A20) | BioLegend | Cat#110724 |
| eFlour780 Fixable Viability Dye | eBioscience | Cat# 65-0865-18 |
| eFluor450 anti-CD4 (Clone: RM4-5) | eBioscience | Cat#48-0042-82 |
| FITC anti-CD25 (Clone: PC61) | BioLegend | Cat#102006 |
| FITC anti-Foxp3 (Clone: FJK-16s) | eBioscience | Cat#11-5773-82 |
| PE anti-CD152(Ctla-4) (Clone: UC10-4B9) | BioLegend | Cat#106306 |
| PE anti-CD4 (Clone: RM4-5) | BioLegend | Cat#100512 |
| PE anti-mouse IgG2a | Jackson ImmunoResearch | Cat#115-115-206 |
| PE Streptavidin | Tonbo Biosciences | Cat#50-4317-U500 |
| PE-Cy7 anti-CD25 (Clone: PC61) | BioLegend | Cat#102016 |
| PE-Cy7 anti-CD62L (Clone: MEL-14) | BioLegend | Cat#104418 |
| Purified anti-CD90.1(Thy1.1) (Clone: HIS-51) | BD Biosciences | Cat#554892 |
| Purified anti-mouse CD3 (Clone: 145.2C11) | Bio X Cell | Cat#BE0001 |
| Purified anti-mouse DC28 (Clone: 37.51) | Bio X Cell | Cat#BE0015 |
| Purified anti-mouse IL-2 (Clone: JES6-54H) | Bio X Cell | Cat#BE0042 |
| Purified anti-mouse IL-2 (Clone: S4B6-1) | Bio X Cell | Cat#BE0043 |
| Rabbit IgG | CST | Cat##2729S |
| **Rabbit mAb anti-histone H3K27ac** | Abcam | Cat#ab4729 |
| Rabbit mAb anti-Stat5 (Clone: D2O6Y) | CST | Cat#94205 |
| Rabbit pAb anti-Foxp3 | Abcam | Cat#ab150743 |
| | | |
| **Chemicals, Kits, and Recombinant Proteins** | | |
| (+)-JQ1 | Sigma-Aldrich | Cat#SML1524 |
| Accel-NGS Methyl-Seq DNA Library Kit | Swift Biosciences | Cat# 30024 |
| BioMag Plus Concanavalin A | Bangs Laboratories, Inc. | Cat#BP531 |
| C646 | Sigma-Aldrich | Cat#SML0002 |
| Click-iT Nascent RNA Capture Kit | Thermo Fisher Scientific | Cat#C10365 |
| Foxp3 / transcription factor staining buffer set | eBioscience | Cat#00-5523-00 |
| I-BET151 | Sigma-Aldrich | Cat#SML0666 |
| I-CBP112 | Sigma-Aldrich | Cat#SML1134 |
| Recombinant human IL-2 | PeproTech | Cat#AF-200-02 |
| Recombinant human TGF-β | R&D Systems | Cat#240-B-002 |
| Recombinant mouse IL-4 | PeproTech | Cat#214-14 |
| Recombinant mouse IL-6 | PeproTech | Cat# 216-16 |
| SGC-CBP30 | Sigma-Aldrich | Cat#SML1133 |
| SPRIselect | Beckman Coulter | Cat#B23318 |
| SuperScript VILO cDNA Synthesis Kit | Thermo Fisher Scientific | Cat# 11754050 |
| | | |
| **Bacterial Strains** | | |
| Stable Competent *E. coli* | NEB | Cat#C3040I |
| | | |
| **Cell Lines** | | |
| Platinum-E | Cell Biolabs, Inc. | Cat#RV-101 |
| | | |
| **Key Equipment** | | |
| CFX384 Real Time System | Bio-Rad | |
| iCyt SY3200 (Synergy) Cell Sorter | Sony | |
| LSR II Flow Cytometer | BD Bioscience | |
| LSR Fortessa Flow Cytometer | BD Bioscience | |

| | | |
|---|---|---|
| M220 Focused Ultrasonicator | Covaris | |
| MoFlo XDP Cell Sorter | Beckman Coulter | |
| | | |
| | | |
| **Deposited data** | | |
| Genome wide bisulfite sequencing | This paper | GSE146250 |
| ATAC-seq | This paper | GSE146250 |
| ChIP-seq | This paper | GSE146250 |
| Cut&Run | This paper | GSE146250 |
| RNA-seq | This paper | GSE146250 |

**Primers for amplicon-based bisulfite sequencing**

| | |
|---|---|
| CNS4-BSC | GATTTTGGGGGTATTGGAATTG |
| | AAATCACTCAACTAATAAATAACCAAACCA |
| Promoter_BSC | GGAGTAGAAGGAAGTTTTTGGAGATAGAG |
| | CTCATAAAAAACCACAATTTCTTAAACAA |
| CNS1-BSC-Set1 | GGTATGGGAGTTAGATTGTTTGGAAT |
| | CACTCTAAAATAATTTCCAAACCCACTAA |
| CNS1-BSC-Set2 | TTAGTGGGTTTGGAAATTATTTTAGAGTG |
| | CACAACATTTCAACATAAAAAACAATACAA |
| CNS2-BSC-Set1 | TTTTGGGTTTTTTTGGTATTTAAGA |
| | ACAAATAATCTACCCCACAAATTTC |
| CNS2-BSC-Set2 | TTTGGGTTTTGTATGGTAGTTAGATG |
| | CACAACCTAAACTTAACCAAATTTTTC |
| CNS3-BSC | GAATTTTTAGGGATTAGGGGTTTTGG |
| | CACCTATAAACCCAAATACCCCACC |

**Primers for ChIP qPCR**

| | |
|---|---|
| CNS4 | AGCAGCACACAGGCCTTAAAAC |
| | GGTTTTCTTTGTAGGTCGGTGAC |
| Foxp3-Promoter | TAATGTGGCAGTTTCCCACAAGCC |
| | AATACCTCTCTGCCACTTTCGCCA |
| CNS1 | AGACTGTCTGGAACAACCTAGCCT |
| | TGGAGGTACAGAGAGGTTAAGAGCCT |
| CNS2 | ATCTGGCCAAGTTCAGGTTGTGAC |
| | GGGCGTTCCTGTTTGACTGTTTCT |
| CNS3 | TCTCCAGGCTTCAGAGATTCAAGG |
| | ACAGTGGGATGAGGATACATGGCT |
| Foxp3-Pro-1.5k | GCAAATGAGGGAAAGAGCAAAG |
| | AGGCCTGAGGAAGAGAAAGTA |
| Exon3 | GATGCCCATGCCCAGAC |
| | GGGCCTTGAGGGAGAAGA |
| 3'UTR1 | CCCAGTGCCCATCCAATAAA |
| | TTCTCCTGCTGGGATCTTAAAC |
| ICOS | TGTATGCTTGCTTTGGTGTTGTG |
| | GTCATGTTGTGGCTTGAGACTGA |

| | |
|---|---|
| Gm5069 | TAAGCAATTGGTGGTGCAGGATGC |
| | AAAGGGTCATCATCTCCGTCCGTT |

**Primers for quantifying RNA via RT-qPCR**

| | |
|---|---|
| Foxp3 | GATGCCCATGCCCAGAC |
| | GGGCCTTGAGGGAGAAGA |
| IL2Ra | AACCATAGTACCCAGTTGTCGG |
| | TCCTAAGCAACGCATATAGACCA |
| Ctla4 | TTTTGTAGCCCTGCTCACTCT |
| | CTGAAGGTTGGGTCACCTGTA |
| Icos | ATGAAGCCGTACTTCTGCCG |
| | CGCATTTTTAACTGCTGGACAG |
| Actin | GGCTGTATTCCCCTCCATCG |
| | CCAGTTGGTAACAATGCCATGT |
| Gapdh | AGGTCGGTGTGAACGGATTTG |
| | TGTAGACCATGTAGTTGAGGTCA |

**Primers for quantifying Tet2 or Tet3 deletion by qPCR**

| | |
|---|---|
| Tet2-KO-F1 | TGGCCACAGTGGAGGTTTACAA |
| Tet2-KO-R1 | AGTGCTTCATGCAAATTCGGGG |
| Tet3-KO-F1 | ATGAGGATGTGGCGATCGACTG |
| Tet3-KO-R1 | GCAGCGATTGTCTTCCTTGGTC |